Electric propulsion for satellites and spacecraft: established technologies and novel approaches

2016 Plasma Sources Sci. Technol. 25 033002

(http://iopscience.iop.org/0963-0252/25/3/033002)

IOP Publishing Plasma Sources Science and Technology

Plasma Sources Sci. Technol. **25** (2016) 033002 (27pp) doi:10.1088/0963-0252/25/3/033002

Topical Review

Electric propulsion for satellites and spacecraft: established technologies and novel approaches

Stéphane Mazouffre

Institut de Combustion, Aérothermique, Réactivité et Environnement (ICARE), CNRS—University of Orléans, 1C avenue de la Recherche Scientifique, 45071 Orléans, France

E-mail: stephane.mazouffre@cnrs-oleans.fr

Received 15 January 2015, revised 9 February 2016
Accepted for publication 15 February 2016
Published 6 April 2016

Abstract

This contribution presents a short review of electric propulsion (EP) technologies for satellites and spacecraft. Electric thrusters, also termed ion or plasma thrusters, deliver a low thrust level compared to their chemical counterparts, but they offer significant advantages for in-space propulsion as energy is uncoupled to the propellant, therefore allowing for large energy densities. Although the development of EP goes back to the 1960s, the technology potential has just begun to be fully exploited because of the increase in the available power aboard spacecraft, as demonstrated by the very recent appearance of all-electric communication satellites. This article first describes the fundamentals of EP: momentum conservation and the ideal rocket equation, specific impulse and thrust, figures of merit and a comparison with chemical propulsion. Subsequently, the influence of the power source type and characteristics on the mission profile is discussed. Plasma thrusters are classically grouped into three categories according to the thrust generation process: electrothermal, electrostatic and electromagnetic devices. The three groups, along with the associated plasma discharge and energy transfer mechanisms, are presented via a discussion of long-standing technologies like arcjet thrusters, magnetoplasmadynamic thrusters, pulsed plasma thrusters and ion engines, as well as Hall thrusters and variants. More advanced concepts and new approaches for performance improvement are discussed afterwards: magnetic shielding and wall-less configurations, negative ion thrusters and plasma acceleration with a magnetic nozzle. Finally, various alternative propellant options are analyzed and possible research paths for the near future are examined.

Keywords: electric propulsion, plasma, low-temperature

(Some figures may appear in colour only in the online journal)

1. Introduction

Electric propulsion (EP) today features a range of mature and well-established technologies for moving satellites and spacecraft in space. The development of EP dates back to the 1960s, with the appearance of plasma sources capable of delivering substantial current [1]. The first in-space demonstrations of EP occurred in 1964 and were achieved with an ion engine aboard the Space Electric Rocket Test (SERT-1) spacecraft and with a pulsed plasma thruster (PPT) aboard the Soviet Zond-2 satellite. Since then, rapid evolutions in EP technology have made possible the emergence of new concepts. EP thrusters have been developed worldwide and hundreds of such thrusters have been operated on satellites and space exploration probes.

However, the full potential of EP has only just begun to be realized, thanks to the increase in the available power on spacecraft, as demonstrated by the very recent appearance of all-electric communication satellites. The revival of the field has also been spurred by future projects that will depend on the deployment of large constellations of EP-powered small satellites.

Like its chemical counterpart, EP relies on the momentum conservation law: a force, called the thrust, is exerted on a space vehicle through the ejection of matter with high kinetic energy. A distinctive feature of EP is that it achieves high propellant exhaust speeds because a large amount of energy, externally stored, can be transferred to the propellant. A large ejection velocity directly translates into a low propellant consumption for a given maneuver. Propellant mass economy is the main advantage of EP with respect to chemical propulsion for which acceleration originates in the conversion of chemical energy into kinetic energy through an expansion process [2–4]. Other advantages of an EP system are the long operation time and flexibility. The current disadvantage of EP is its very low thrust level, which is related to the power source limitation, as we shall see. EP technologies may be split into three broad categories according to the way thrust is generated: electrothermal, electrostatic and electromagnetic propulsion. These groups encompass numerous approaches and devices that cover a vast range of characteristics and performances. The inclined reader can find several textbooks and review articles about EP; see e.g. [3–12]. This study aims at contributing to the EP literature not only by describing the fundamentals of the field and the physics of well-established and mature technologies, but also by presenting novel approaches and concepts and by explaining propellant choice, a key concern for a thruster assembly. This review article solely focuses on devices and solutions for moderate and high thrust levels; it does not deal with micropropulsion technologies for cubesat, nanosat and missions that require very precise positioning, like field emission electric propulsion, colloid thrusters, ionic liquid electrospray thrusters and miniaturized versions of devices described in this review. An example of application is the LISA Pathfinder mission for gravitational wave detection for which the spacecraft uses colloid thrusters for drag-free control [13]. Note that a critical issue in some micropropulsion devices is the decrease in efficiency due to increasing wall-losses.

The paper is organized as follows. In section 2 the physical background of EP is presented along with the relevant figures of merit. The impact of the power source on the mission profile is also discussed. Section 3 gives the principle and the performances of long-standing technologies, i.e. resistojets, arcjet thrusters, magnetoplasmadynamic (MPD) thrusters, PPTs and derivatives. Gridded ion engine operation and characteristics are described in section 4. The recently developed annular geometry ion engine is also presented. Section 5 outlines the Hall thruster (HT). The physics at play are analyzed and remaining challenging issues are discussed. The variants of the HT are also briefly described. Section 6 is devoted to novel approaches and advanced concepts. The magnetic shielding and wall-less configurations of HTs are compared to the standard design. The negative ion thruster technology is introduced with emphasis on ion–ion plasma creation and challenges posed by ion pair acceleration. Finally, electrodeless devices, which are based on the expansion of a plasma through a solid or a magnetic nozzle (radiofrequency and helicon thrusters, microwave thrusters and the VASIMR engine), are discussed. The mechanisms at the origin of thrust generation with a magnetic nozzle, i.e. plasma acceleration and detachment, are explained at the end of section 6. The numerous criteria for choosing a suitable propellant for an EP assembly are listed in section 7. The analysis reveals that only a few candidates are feasible alternatives to xenon. Finally, general conclusions are drawn in section 8 and perspectives are given to end this review.

2. Fundamentals of EP

2.1. Ideal rocket equation

The motion of a space vehicle is governed by the law of action–reaction or momentum conservation principle. The acceleration is created by the expulsion of a propellant mass [2–4]. We consider a rocket of mass m moving at velocity $\mathbf{v}$ and subject to external forces $\mathbf{F}_{\text{ext}}$. The rocket mass decreases at a rate $\dot{m} = \mathrm{d}m/\mathrm{d}t$. Applying Newton's second law to the rocket between times t and $t + \mathrm{d}t$ leads to the general equation of motion for a variable mass system

$$\mathbf{F}_{\text{ext}} + \frac{\mathrm{d}m}{\mathrm{d}t}\mathbf{v}_{\text{e}} = \mathbf{F}_{\text{ext}} + \dot{m}\mathbf{v}_{\text{e}} = m\frac{\mathrm{d}\mathbf{v}}{\mathrm{d}t}, \tag{1}$$

where $\mathbf{v}_{\text{ext}}$ is the velocity vector of the ejected propellant mass relative to the rocket. The product $\mathbf{T} = \dot{m}\mathbf{v}_{\text{e}}$ is called the thrust of the rocket. It can be interpreted as an additional force applied to the rocket due to expulsion of the propellant. Projecting all vectors along the direction of the velocity $\mathbf{v}$, neglecting external forces such as gravity, drag and radiation pressure, and assuming the magnitude of the exhaust velocity $\mathbf{v}_{\text{e}}$ is constant, the previous equation can be integrated in time to give an expression for the change in velocity Δv

$$\Delta v = v_{\text{f}} - v_0 = v_{\text{e}} \ln\left(\frac{m_0}{m_{\text{f}}}\right) = v_{\text{e}} \ln\left(1 + \frac{m_{\text{p}}}{m_{\text{f}}}\right), \tag{2}$$

where the subscripts 0 and f refer to the initial time t_0 and the final time t_{f} of the acceleration period, respectively. The initial mass m_0 is the sum of the propellant mass m_{p} consumed during the propulsion time $t_{\text{p}} = t_{\text{f}} - t_0$ and the final burnout mass m_{f}, which includes the dry mass and the payload mass to deliver. Equation (2) is known as the ideal rocket equation, or the Tsiolkovsky rocket equation after the Russian physicist who first derived it in 1903. It relates the change in velocity, or velocity increment, Δv of a spacecraft to the propellant ejection speed, the propellant mass and the final mass [2, 3]. The rocket equation shows there are two options to achieve a large Δv: either to burn a substantial amount of propellant ($m_{\text{p}} \approx m_0$) or to use a thruster able to generate a high v_{e}. The second option is preferable since it allows a bigger and heavier payload. The necessary Δv to perform a maneuver or to accomplish a mission can be computed from

Table 1. Typical Δv for various maneuvers and missions (LEO: low-Earth orbit; GEO: geosynchronous orbit; Lx: Lagrangian points).

Satellite displacement	Δv (m s^{-1} per year)
Drag compensation (500 km)	30
Attitude control	2–6
Station keeping in GEO	50
Orbit transfer	**Δv (km s^{-1})**
Earth—LEO	9,7
LEO—GEO	4,3
LEO—Moon	5,9
LEO—L1	3,7
LEO—L2	3,4
LEO—Mars	4,3
Interplanetary journeys	**Δv (km s^{-1})**
Nearby planets	5–8
Far-off planets	10–15
100–1000 au	100
10 000 au	1000
Interstellar medium	30 000

Note: The symbol au refers to the astronomical unit, which is roughly the distance from the Earth to the sun (1 au = 149 597 871 km).

orbital mechanics. Some typical Δv for various maneuvers and space trips are listed in table 1 [14]. The range of Δv is very broad and the magnitude reaches several tens of km s^{-1} for exploration of the solar system. As the velocity increment is a known quantity given a space mission scenario, a more appropriate form for equation (2) is the one that is expressed in terms of propellant mass

$$m_{\mathrm{p}} = m_0\left[1 - \exp\left(\frac{-\Delta v}{v_{\mathrm{e}}}\right)\right]. \tag{3}$$

In order to reduce the propellant consumption, or, in other words, in order to deliver a significant payload mass to its destination, the exhaust velocity must at least be comparable to, or better, larger than, the velocity increment. Figure 1 shows the evolution of the m_{p}/m_0 ratio with the exhaust speed v_{e} for two velocity increments. A high exhaust speed allows us to drastically reduce the propellant fraction, which translates into cost reduction or improvement of the mission characteristics, e.g. larger payload or increased duration. Chemical thrusters, whether liquid or solid, are fundamentally limited by the energy per unit of mass stored in the propellant, in such a way that v_{e} cannot exceed 5500 m s^{-1} [2, 3]. This limitation can be circumvented by changing the energy conversion mechanism: the energy source must be separated from the propellant. EP, like nuclear propulsion and beam propulsion [3, 4], is one possibility as an external energy source is used to energize and to accelerate the propellant, as we shall see later. EP therefore allows high v_{e} making possible missions with large Δv unaffordable with chemical engines.

2.2. Specific impulse

The total impulse $\mathbf{I}$ is defined as the integral of the thrust over the operating duration of the thruster

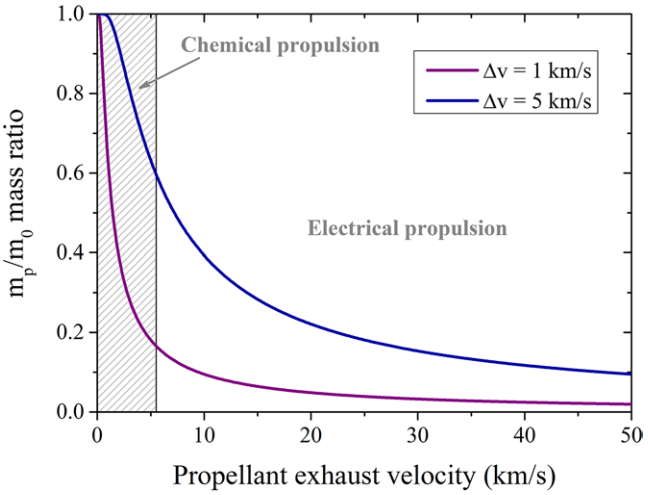

Figure 1. Ratio of the propellant mass to the initial mass as a function of the exhaust velocity v_{e} for two values of the velocity increment Δv. The dashed area corresponds to the domain of chemical propulsion with v_{e} below 5.5 km s^{-1}.

$$\mathbf{I} = \int_0^{t_{\mathrm{p}}} \mathbf{F}(t)\mathrm{d}t = \int_0^{t_{\mathrm{p}}} \dot{m}_{\mathrm{p}}\mathbf{v}_{\mathrm{e}}\mathrm{d}t = m_{\mathrm{p}}\mathbf{v}_{\mathrm{e}}, \tag{4}$$

where $\dot{m}_{\mathrm{p}}$ is the propellant mass flow rate. The exhaust speed is assumed constant in equation (4). The total impulse measures the change in momentum that a thruster can impart to a rocket or a spacecraft. It is expressed in Ns. Equation (4) indicates that there are two ways to reach a certain impulse: either a strong force is applied during a short time period or a weak force is applied during a long time period. The second strategy corresponds to the EP, which allows us to achieve a long propulsion time thanks to a low propellant consumption, while the thrust level stays moderate due to power constraints.

The specific impulse I_{sp} is the impulse delivered per unit of propellant consumed. It is equivalent to the thrust produced per unit of propellant flow rate. The I_{sp} is defined by convention in terms of weight at the surface of the Earth; it is therefore expressed in seconds

$$I_{\mathrm{sp}} = \frac{\int_0^{t_{\mathrm{p}}} F(t)\mathrm{d}t}{g_0\int_0^{t_{\mathrm{p}}} \dot{m}_{\mathrm{p}}\mathrm{d}t} = \frac{I}{g_0 m_{\mathrm{p}}}, \tag{5}$$

where g_0 is the standard gravity of the Earth. If the thrust is constant, which is true if the ignition and shutdown stages are neglected, then the I_{sp} is simply proportional to v_{e}

$$I_{\mathrm{sp}} = \frac{F}{g_0\dot{m}_{\mathrm{p}}} = \frac{v_{\mathrm{e}}}{g_0} \approx \frac{v_{\mathrm{e}}}{10}. \tag{6}$$

The specific impulse is a relevant figure of merit in the field of space propulsion as it is a measure of the efficiency of a thruster in terms of fuel consumption. As can be seen in equation (5), the higher the specific impulse, the less propellant is needed to produce a given impulse level. The high I_{sp} of electrical thrusters make them very attractive as long as the length of time is not a critical aspect for the mission. Due to a high I_{sp}, EP allows us to achieve a large spacecraft final velocity and a large total impulse provided that the thruster

Table 2. Characteristics of various electrical power sources for EP. RTG stands for radioisotope thermoelectric generator.

Property	Electrical power source			
#	Solar panels	Batteries/fuel cells	RTG	Nuclear reactor
Power (kW)	1–15	0,1–100	0.1–1	100–1000
Efficiency (%)	20–30	>90	<7	30
ξ (W kg^{-1})	150–300	100–1000	5	5–40
Degradation	High	Low	Medium	Low
Orbit	Earth	Interplanetary	Interplanetary	Interplanetary

Note: The mean solar energy near the Earth is 1360 W m^{-2} (600 W m^{-2} around Mars and 50 W m^{-2} around Jupiter).

is fired during a long enough time period. The lifetime of the propulsion system, which is mostly governed by erosion and deterioration of components such as the plasma chamber, electrodes and the neutralizer, therefore becomes an essential parameter. Consequently, the EP technology must be highly reliable with a very low failure probability over a long time span.

2.3. Efficiency

In many efficient EP devices atoms or molecules of the input propellant, which can be in a solid, liquid or gaseous state, must first be converted into ions before being accelerated to high velocity and ejected outwards. As only a fraction of the stored propellant is transformed and produces thrust, an essential quantity is the mass or propellant utilization efficiency

$$\alpha = \frac{\dot{m}_\mathrm{i}}{\dot{m}_\mathrm{p}} = \frac{I_\mathrm{b}}{e}\frac{M}{\dot{m}_\mathrm{p}}, \tag{7}$$

where $\dot{m}_\mathrm{i}$ is the ion mass flow rate, I_b is the ion current in the exhaust beam, e is the elementary charge and M is the propellant atomic mass. Equation (7) is given assuming the exhaust beam only contains singly-charged ions, but the mass utilization efficiency can easily be corrected to account for multiply-charged ion species [6, 16]. Hence for thrusters in which the propellant is ionized the thrust reads $T = \dot{m}_\mathrm{i} v_\mathrm{e} = \alpha \dot{m}_\mathrm{p} v_\mathrm{e}$ and the specific impulse is given by $I_\mathrm{sp} = \alpha \frac{v_\mathrm{e}}{g_0}$. In fact $\alpha = 1$ has two meanings in EP: either the propellant flow is fully ionized, which demonstrates a high efficiency, or the thrust production mechanism does not rest on the acceleration of ions. Instead, the propellant is electrically heated and expanded into the vacuum, as we shall see later. As α is a quantity that is difficult to accurately determine, the mechanical power in the beam is usually not used as a performance indicator to compare technologies. Instead, the thrust efficiency η of any electrical thrusters is defined as

$$\eta = \frac{P_\mathrm{mecha}}{P_\mathrm{elec}} = \frac{\dot{m}_\mathrm{p} v_\mathrm{e}^2}{2P_\mathrm{elec}} = \frac{T^2}{2\dot{m}_\mathrm{p} P_\mathrm{elec}}, \tag{8}$$

where P_elec is the input electrical power. With this definition, η can be accessed by measuring the thrust in a test chamber. The previous equation is also valid for chemical thrusters by replacing P_elec with the available chemical power. To reach a high thrust efficiency, all power loss terms must be minimized; they encompass fuel ionization and dissociation, velocity spread, beam divergence, power deposition at walls and on the electrodes, radiation and losses in components like the neutralizer and magnetizing coils.

Equation (8) can be used to express the thrust per unit input power or thrust-to-power ratio

$$\frac{T}{P_\mathrm{elec}} = \frac{2\eta}{\alpha v_\mathrm{e}} = \frac{2\eta}{g_0 I_\mathrm{sp}}. \tag{9}$$

As can be seen, the thrust level is limited by the available onboard power. Moreover, for a fixed input power and thrust efficiency, increasing the I_sp reduces the thrust. There is therefore a trade-off between T and I_sp, even if $\eta = 1$. As electrical thrusters deliver a high specific impulse, they are low-thrust devices operating during long periods of time.

2.4. Power source constraint

In electrical propulsion, the energy is supplied from an external source, which means the propellant and energy necessary to create momentum are uncoupled, in contrast to chemical propulsion. The power can be generated from several types of source like photovoltaic solar panels, batteries, an RTG or a nuclear reactor [3, 15]. Advantages and drawbacks of the various sources are summarized in table 2. Two criteria are of particular relevance for spaceflight: the output power and the source mass [3, 7]. The total power available on board the spacecraft directly determines the thrust level, as shown by equation (9). For instance, to produce 10 N (≈1 kg) with an efficiency of 50% and an I_sp of 3000 s (typical values for EP systems) requires 300 kW of electrical power, which would necessitate a solar panel area of about 900 m^2 near the Earth, according to table 2. Furthermore, the power supply must be carried by the space vehicle. Contrary to a chemical rocket, the mass of the energy source of an electrical rocket does not decrease in time. It corresponds to a dry mass. As a consequence, the power-to-mass ratio ξ of the source appears to be a critical parameter. Data in table 2 show that solar arrays and batteries are the most suited energy sources for EP. Light and high-yield batteries are not yet ready for in-space propulsion applications, therefore electrical thrusters are currently powered with solar panels. Efficiency increase and mass reduction of solar panels are however needed for ambitious exploration missions towards asteroids and nearby planets. For interplanetary journeys towards far-off planets, the nuclear fission reactor remains the best option so far [3, 4, 14].

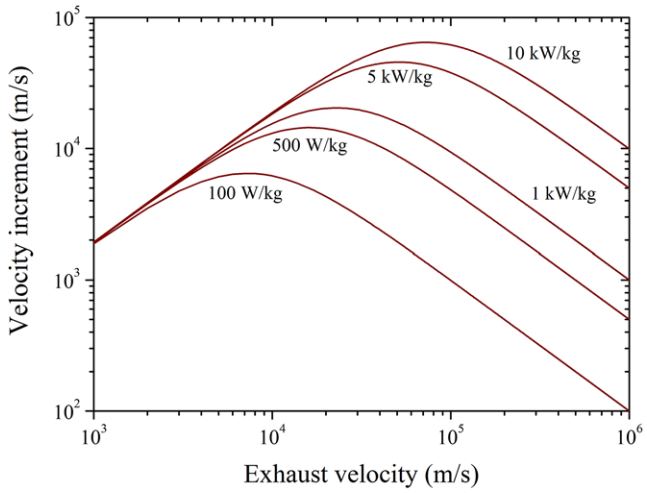

Figure 2. Δv against exhaust velocity v_e for many values of the power-to-mass ratio ξ ($m_s/m_p = 0.17$, $\eta = 0.5$, $\alpha = 1$ and $t_p = 280$ h).

It is apparent from the above that the exhaust velocity as well as the thrust depends on the mass of the power source [8]. Using equation (9) and introducing ξ, the thrust of an electrical propulsion device becomes

$$T = \dot{m}_i v_e = \alpha \dot{m}_p v_e = \sqrt{\frac{2\eta\xi m_p m_{elec}}{t_p}}, \qquad (10)$$

where m_{elec} is the mass of the power supply. The need for a large thrust efficiency and a high power-to-mass ratio is well exemplified in the preceding equation. For fixed values of η and ξ, increasing the thrust requires an increase in the power supply mass, with penalty on the mission objectives. As the mass of the power source counts as dry mass for an EP system, the classical Tsiolkovsky equation is no longer suitable. A more sophisticated equation must be used instead [3]. A possible form is the following

$$\Delta v = v_e \ln\left(1 + \frac{2\eta\xi t_p}{2\eta\xi t_p \frac{m_s}{m_p} + \alpha^2 v_e^2}\right), \qquad (11)$$

where the structure mass m_s includes the payload mass. The velocity increment Δv is plotted as a function of v_e for several values of the power-to-mass ratio ξ in figure 2. The figure clearly shows the spacecraft velocity does not increase monotonically with v_e. A large v_e requires a great amount of power, which means a heavy power supply. When the mass of the power unit becomes large compared to the vehicle dry mass, the Δv decreases. A higher ξ increases the achievable velocity increment and the peak Δv moves towards larger v_e as ξ increases. The propulsion time t_p can of course be adjusted to reach a large Δv but this creates constraints on the mission profile. When designing an EP-based space mission, the thruster, wherein thrust and I_{sp} are produced, cannot be separated from its power supply, as illustrated in this paragraph. The power-to-mass ratio of the power unit is then a key element to obtain the best performance and to optimize the mission scenario.

2.5. Electric thruster classification

As previously explained, the basic principle of EP consists of applying electrical energy to the propellant from an external power source to achieve a high exhaust speed well above what a chemical engine produces. The conceptual classification of electric thruster concepts and technologies is defined according to the way the electrical energy is transferred (plasma production) and the thrust and I_{sp} are generated (plasma acceleration). The EP field is therefore divided into three broad categories [7, 17]:

– *Electrothermal propulsion*
Electricity is used to heat the propellant in a chamber. Expansion of the hot neutral or ionized gas through a suitable nozzle allows conversion of the thermal energy into kinetic energy, which imparts momentum to the spacecraft.

– *Electrostatic propulsion*
Electrical power is first used to ionize the propellant. Ions are subsequently accelerated by means of electrodes by the direct application of an electric field.

– *Electromagnetic propulsion*
The propellant is ionized and accelerated under the combined action of electric and magnetic forces.

Table 3 provides some characteristics of standard electrical thrusters for spacecraft. It encompasses the three categories of EP systems. For comparison, the properties of the three types of chemical engines are also given in table 3. As previously explained, chemical thrusters can generate a tremendous thrust level, which is required for launchers, though during a short time period due to the limited I_{sp}. In a chemical rocket the specific impulse originates from the conversion of thermal energy into kinetic energy during expansion of the gas through a nozzle [2, 3]. The simplified approach of a free isentropic expansion shows the exhaust velocity is related to the sound speed c_s in the chamber

$$v_e \leqslant c_s \sqrt{\frac{2}{\gamma - 1}} = \sqrt{\frac{2\gamma}{\gamma - 1}\frac{k_B T}{m}}, \qquad (12)$$

where γ is the specific heat ratio of the gas, k_B the Boltzmann constant, T the temperature upstream of the nozzle throat and m the atomic mass of the propellant. The I_{sp} therefore depends both on the propellant thermodynamic properties and on the temperature. EP offers two strategies to circumvent the limitations illustrated by equation (12): where the propellant can be heated to a very high temperature an *electrothermal* approach can be taken; where the kinetic energy production does not rest on a thermal process an *electrostatic/electromagnetic* approach can be taken.

3. Long-standing technologies

3.1. Resistojets—arcjets

A resistojet generates thrust by heating a fluid using the Joule effect [5, 7, 8]. The principle is illustrated in figure 3(a). The

Table 3. Typical performance data and standard propellant for various types of chemical and electrical thrusters.

Thruster type	I_{sp} (s)	Thrust (N)	Power (kW)	Propulsion time	Fuel
Chemical					
Cold gas	50	0.1–100	0.05	∼mn	N_2, ammonia
Liquid	200	1–500	10^2	∼h	hydrazine
Liquid	300–400	10^6	10^7	∼mn	$LO_2 + H_2$, kerosene
Solid	250	10^7	10^8	100 s	powder (Al, Mg, Zn, S)
Electrothermal					
Resistojet	100–300	0.2	0.1–1	∼h	N_2, hydrazine, Xe
Arcjet	500	0.1	1	1000 h	hydrazine, ammonia
Electrostatic					
Gridded ion engine	3000	10^{-3}–0.1	0.1–5	30 000 h	Xe
Electromagnetic					
Hall thruster	1500	10^{-2}–1	0.2–20	10 000 h	Xe
MPD thruster[a]	1000–10 000	0.5–50	100–10^3	1000 h	Ar, H_2, Li
Ablative PPT[b]	500–1500	10^{-5}–10^{-2}	0.01	1000 h	PTFE

[a] Both self-field and applied-field magnetoplasmadynamic thrusters are considered.
[b] The thrust level depends upon the repetition rate; the impulse bit is typically 500 μN s.

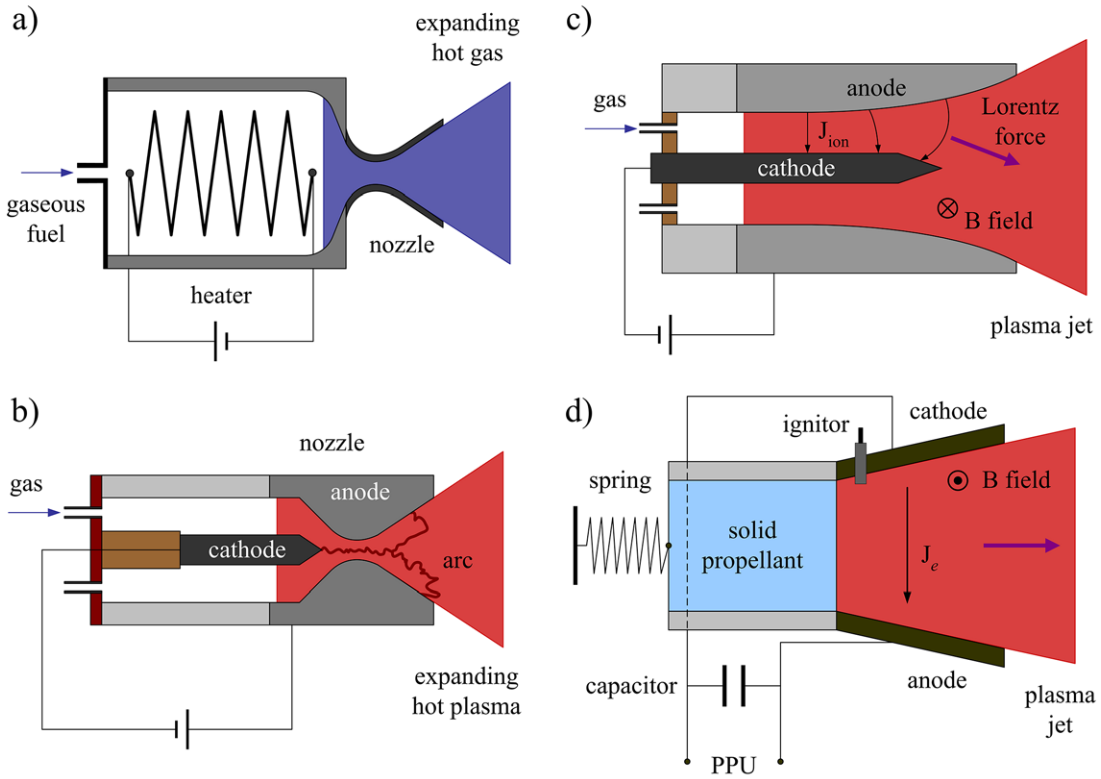

Figure 3. Schematic of electrothermal and electromagnetic thrusters: (a) resistojet, (b) arcjet thruster, (c) self-field MPD thruster and (d) ablative pulsed plasma thruster.

gas is first heated electrically, passing through resistance heaters of various geometries (solenoid, rods, plate). The hot gas is subsequently expanded through a convergent–divergent solid nozzle to create thrust. The specific impulse therefore increases as $\sqrt{T}$; see equation (12). All gaseous propellants can be used, but they must be compatible with the heater material. The temperature in the resistojet chamber is constrained to about 3000 K due to the wall material properties. The I_{sp} is then around 300 s, which is well above what is achieved with a cold gas thruster with a small increase in complexity and a high efficiency above 50%. Although resistojets have a low I_{sp} level, they are attractive because they can be easily integrated, they use the propellant management system of chemical thrusters and they operate at low voltage, which does not necessitate complicated power conditioning equipment. In addition, resistojets are low-cost, reliable and safe devices. For these reasons they are particularly well suited for small satellites and they were among the first electric options for propulsion of communication satellites [5]. Note that it is the only EP technologies which do not involve the plasma state.

The arcjet is another form of thermal engine for spacecraft propulsion [3, 8, 18, 19]. The purpose is to overcome the temperature limitation of a resistojet by passing an electrical arc directly through the gas flow. Figure 3(b) shows a layout of arcjet thruster cylindrical architecture. A high-current arc (∼100 A) is created between the conical tip of a rod, which acts as a cathode, and a divergent nozzle that serves as an anode. The two electrodes are made of tungsten that has a high melting point. Thorium is often incorporated into the cathode material to enhance electron emission. A steady DC potential of about 100 V is established across the anode–cathode gap. The gas is injected in the region upstream of the nozzle throat. A high-density high-temperature thermal plasma is produced in the throat; however, a large fraction of the gas flow remains neutral [20, 21]. The temperature in the core of the plasma reaches 1–2 eV. A strong gradient in the radial direction keeps the wall temperature around 2000 K. Atoms are heated by collision events with electrons and ions [20]. The hot gas expands through the nozzle, where thermal energy is converted into kinetic energy. In order to attain a high efficiency, the energy must be transferred to the neutrals before the expansion process begins. Typically, the efficiency of an arcjet thruster is 30%, which is below the efficiency of a resistojet. However, the increase in I_{sp} is noticeable.

Arcjets operate under standard conditions at an input power level of a few kW [8, 18, 19, 22]. The usual propellant is either ammonia or hydrazine. The specific impulse is therefore around 500 s. An I_{sp} level above 1000 s was achieved with hydrogen and helium [23, 24]. Low-power arcjet thrusters operating at around 100 W have also been developed for micro-satellites [25]. Water-cooled arcjets were also operated at 100 kW during short periods here on Earth, with a thrust level up to 4 N [23]. The lifetime of the device is only a few hundreds of hours. It is determined by erosion and evaporation of the cathode material under ion bombardment in the arc area, especially at discharge ignition. The relatively short lifetime and the unstable character of the arc plasma are the main handicaps of arcjet thrusters.

3.2. MPD thrusters—PPT

The thermal expansion process limits the specific impulse to moderate values, even with light propellants. The only way to increase the I_{sp} level and the thrust density is to turn towards magnetic and electric interactions instead. A self-field MPD thruster, see figure 3(c), is a plasma accelerator composed of two concentric electrodes between which a very high current discharge is established [5, 7, 26, 27]. The anode-to-cathode potential is relatively low, between 50 V and 300 V. The anode acts as a nozzle for plasma acceleration. It also dissipates thermal energy. The nozzle geometry has a great influence on the MPD thruster performance and several studies have been performed using numerical simulations to optimize the design; see e.g. [28, 29]. The gaseous propellant, which is injected into the upstream part of the device, is ionized by electron impacts. A magnetic Lorentz force density $\mathbf{F}_L = \mathbf{j} \times \mathbf{B}$ in N m^{-3}, which results from the interaction between the radial current density $\mathbf{j}$ flowing through the plasma and the self-induced magnetic field $\mathbf{B}$ in the azimuthal direction, accelerates the plasma to high exhaust velocities in the axial direction, as depicted in figure 3(c). In an MPD thruster, the thrust mostly originates from the combination of the gradient of the plasma thermal pressure p along with the gradient of the magnetic pressure $B^2/(2\mu_0)$, where μ_0 is the vacuum permeability. The effect of the neutral gas pressure is negligible. The regime of operation of an MPD thruster is therefore controlled by the plasma β parameter that corresponds to the ratio of the thermal to the magnetic pressure [10]

$$\beta = \frac{2\mu_0 p}{B^2}. \tag{13}$$

As the induced magnetic field is proportional to the discharge current I_d, the magnetic pressure is weak at low I_d. In that case, an MPD thruster operates mainly as an electrothermal device. An MPD thruster is efficient, i.e. the ionization degree is high and the thrust density is large, in a low β regime: $\beta \leqslant 1$. The transition between the two β regimes of an MPD thruster is well observed in experiments as the slope of the current–voltage curve changes abruptly from a linear behavior to a power law ($V_d \propto I_d^3$) [30, 31]. The need for a high discharge current is well illustrated through some numbers. Considering a plasma density $n_e = 10^{21}$ m^{-3} and an electron temperature $T_e = 4$ eV, an azimuthal magnetic field strength of 570 G is then necessary to reach $\beta = 0.5$. Assuming an MPD device with a 2 cm electrode gap, the discharge current goes up to 5700 A. As a consequence, the power level lies in the MW range. Therefore an MPD thruster must be regarded as a very high power option for spacecraft propulsion. The thrust produced by an MPD thruster is proportional to I_d^2 in the electromagnetic (low β) regime [8, 10, 26]. The specific impulse scales consequently as the ratio $I_d^2/\dot{m}$.

MPD thrusters are simple, robust and compact devices. They have the capability of generating steady-state thrust densities as high as 10^5 N m^{-2}, whereas state-of-the-art HTs and gridded ion engines generate ≈50 N m^{-2} and ≈10 N m^{-2}, respectively, when using Xe as fuel. MPD thrusters produce thrust between 0.5 and 50 N and they provide specific impulses in the 1000–10 000 s range with a thrust efficiency approaching 40% when operating with H_2, He or Ar [27, 32–34]. The low thrust efficiency of MPD thrusters originates in the high ionization cost of the propellant, losses in the electrode sheath and residual thermal energy accumulated in the flow [8]. The lifetime of MPD engines is restricted by erosion and evaporation of the cathode material and it does not exceed 1000 h. In addition, the input power level of MPD thrusters is bounded by the appearance of discharge instabilities and severe electrode erosion at very high power. Various complementary theories have been suggested for explaining this unstable and inefficient operating regime, such as anode sheath collapse, full ionization of the gas and current-driven instabilities [10]. Although MPD thrusters are very attractive from a thrust and I_{sp} standpoint, they remain complicated propulsion systems in terms of their underlying physical mechanisms with a moderate energy efficiency and a short operational life. Moreover, their development and space fight qualification

require large and expensive vacuum test chambers with enormous pumping capacity that are currently rare [35], which creates formidable technological challenges. There are, however, interesting and promising paths for improving the overall performance of self-field MPD thrusters. Firstly, the electrode and nozzle geometry can be optimized to decrease the deposition of power into the anode [28, 29]. Another option consists of replacing the standard tungsten rod cathode with a set of hollow cathodes with low work-function inserts in order to extend the system lifetime. High thrust efficiencies and lifetime elongation have been attained by using propellants with a low ionization energy such as alkali metals. The Lithium Lorentz Force Accelerator (Li-LFA) is a steady-state MPD thruster fueled with lithium [36]. The first ionization energy of Li is 5.4 eV compared to 15.8 eV and 12.1 eV for Ar and Xe, respectively. The Li-LFA thruster has demonstrated erosion-free operation at moderately high power levels (≈200 kW) while delivering up to 12.5 N and 4000 s with an efficiency close to 50% [32]. Finally, MPD thrusters can also be operated in pulsed mode with a long pulse duration to generate a quasi-steady acceleration [5, 34, 37]. This approach allows us to combine the advantages of MPD thrusters with the limited power aboard spacecraft. Even though the MPD thruster technology is not yet entirely mature, its specific features as regards thrust and I_{sp} make it particularly attractive for high Δv missions that necessitate large thrust levels such as cargo transport to the moon and Mars, robotic and crewed missions to Mars and the far-off planets, and deep-space exploration [4]. In addition, MPD thrusters are well suited for large platform orbit transfer in the Earth's vicinity [38]. A last point worth mentioning is that as MPD thrusters require hundreds of kW of power to operate efficiently, their implementation is strongly connected with the development and building of nuclear reactors for spacecraft.

A variant of the self-field MPD thruster is obtained by superimposing a steady longitudinal magnetic field to the induced field. The additional **B** field is created either by magnetizing coils or permanent magnets. This propulsion device is called an applied-field MPD (AF-MPD) thruster [5, 8, 39, 40]. The applied magnetic field is at the origin of azimuthal currents that create axial and radial magnetic Lorentz forces. The axial component accelerates the plasma while the radial component mainly confines the plasma. Two power regimes must be distinguished for AF-MPD thruster operation. The addition of an axial **B** field improves the performances of MPD thrusters at very high power. For instance, the Li-LFA thruster achieved its best performances in AF mode [32]. At low power, the self-induced field is negligible compared to the applied field, and the AF-MPD thruster must be considered as a separate thruster type. In an AF-MPD thruster a high-density hot plasma is produced in the chamber and it expands through a magnetic nozzle formed by the diverging magnetic field, which generates thrust and I_{sp}. In AF configuration, a low-power MPD thruster must therefore be categorized as an electrothermal thruster. Such devices exhibit higher performances at power levels between 10 and 200 kW [41, 42].

PPTs are electromagnetic-type plasma accelerators that offer two distinctive features compared to other concepts [43–45]: they operate in short pulse mode (≈10 μs) and they employ a solid propellant that is consumed in an ablative discharge in their most advanced form, although liquid propellants are gaining attention as they can be supplied easily [46, 47]. Figure 3(d) shows the basic arrangement of an ablative PPT. The only moving part is the spring that passively pushes the propellant for replenishment. The discharge is ignited between the two electrodes by means of a high-voltage pulse applied to a spark plug. Once initiated, the PPT discharge turns into an arc (≈100 V, ≈10 kA) thanks to the energy stored in the capacitor (>10 J). The high-current short-duration (≈10 μs) discharge ablates and ionizes a small amount of solid propellant, which is then accelerated to high velocity. The pulse repetition rate of a PPT is typically of a few Hz. Similarly to MPD thrusters, the thrust in PPT has two components. The self-induced magnetic field due to the high instantaneous current generates a magnetic Lorentz force responsible for the high I_{sp} level. The second component arises from the thermal expansion of the hot plasma ($T_e > 1$ eV). Performances of PPT are affected by various factors: the electrical circuit, the thruster design, the pulse waveform, the nozzle geometry and the propellant [43, 45]. The propellant of an ablative PPT must be nontoxic, inert, dielectric and easy to ablate and ionize. Although many polymers have been evaluated, polytetrafluoroethylene (PTFE) is currently the preferred option. Typical performances of ablative PPT are summarized in table 3. The I_{sp} ranges between 500 and 1500 s. The instantaneous thrust is very large (several N) but the steady-state thrust is low as the device operates in pulsed mode. A more suited parameter is therefore the impulse bit I_{bit}, which is the change in momentum per pulse, or in other words, the integral of the thrust during the pulse duration [43, 44, 48]

$$I_{bit} = \int_0^\tau T(t)\mathrm{d}t = T\ \tau = m_{bit}\ I_{sp}\ g, \qquad (14)$$

when the thrust is constant during the pulse duration τ. In the above equation, m_{bit} is the mass ablated during one shot. The impulse bit of a PPT is below 0.1 mN s. Equation (14) allows us to link the thrust efficiency η to the impulse bit: $\eta = I_{bit}^2/(2m_{bit}E)$, where E is the energy released by the capacitor per cycle. The efficiency of a PPT is thus far below 10% due to the incomplete utilization of the propellant combined with a large electrothermal contribution, especially at low power levels [44, 49]. The PPT was the first EP technology to be used in space aboard the Soviet satellite Zond-2 in 1964. PPTs are simple, compact and robust low-power solid-state thrusters that offer high specific impulse, precise impulse bit control and throttling capability by varying the repetition rate. They currently appear as an attractive option for accurate attitude control, station-keeping and primary propulsion of power-limited microsatellites (<500 kg).

Several research paths have emerged to increase PPT performances and to extend the power range without compromising the advantages of the technology. The solid propellant can be replaced by a gaseous propellant to favor the electromagnetic acceleration [50]. A gas-fed PPT could in principle deliver I_{sp} above 10 000 s. An ablative PPT can be operated in Z-pinch configuration to increase the thrust-to-power ratio

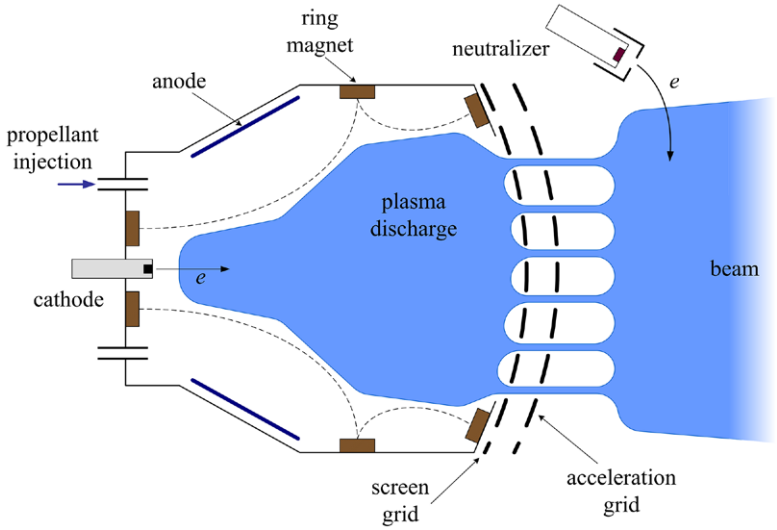

Figure 4. Schematic diagram of a DC electron bombardment GIE with two grids. A GIE is composed of three main elements: the ion source (DC, RF, μ-wave), the acceleration stage with grids and the neutralizer.

and the propellant utilization [51]. Inductively coupled pulsed thrusters have been investigated as a possibility to limit the interaction between the electrodes and the plasma, hence mitigating the lifetime issue [52, 53]. Another possibility to improve PPT efficiency is to use metals as a propellant. This approach has led to the development of the vacuum arc plasma thruster [54–57]. Such devices rest on the production of fully ionized micro-plasmas on the cathode surface, which subsequently expand into the vacuum, producing thrust.

4. The gridded ion engine

4.1. Architecture and operation principle

The gridded ion engine (GIE), or ion thruster, is an example of an ion accelerator in which the thrust density is achieved through electrostatic interactions: $(\varepsilon_0/2)E^2$, where ε_0 is the permittivity of free space and E is the electric field [6]. With the electric field magnitude practical today, the theoretical thrust density is $\approx$100 N m^{-2}. The development of GIE started in the 1960s [1, 5], and this technology is nowadays mature with a long flight heritage. Many detailed articles about the physics, the limitations and applications of ion engines have been published; see e.g. references [3, 5, 6, 58–61]. Here, we only propose an overview of the working principles with emphasis on ion production methods and thrust generation.

The propellant ionization and ion acceleration processes are physically separated in a GIE, contrary to the thrusters previously described. This special feature permits a fine tuning of thrust and exhaust velocity. The gas is injected and ionized in an isolated chamber, as illustrated in figure 4. The chamber geometry can be cylindrical, spherical, semi-spherical and even spheroidal. GIEs are classified according to the way electrical energy is transferred to the gaseous propellant [62]. In DC mode, ions are created by direct electron impact, with the energetic primary electrons (10–50 eV) furnished by a hollow cathode placed in the chamber [5, 58, 59]; see figure 4. Electrons are magnetically confined using a weak field in ring cusp configuration to increase their residence time, hence increasing the ionization degree. This type of electron bombardment ion source is often referred to as a Kaufman source [62]. Ionization can be achieved by means of waves as well. An external inductive coil wound around the thruster body can inductively couple a radiofrequency (RF) wave to the plasma [60–66]. The energy is then deposited close to the dielectric walls in a narrow region of the size of the electron skin depth where an evanescent electric field exists. RF ion engines offer several advantages with respect to DC engines despite a slightly lower thrust efficiency: the internal cathode is not required, magnetic confinement is unnecessary and the erosion of the chamber is reduced. A plasma can be efficiently heated by superimposing a static magnetic field (>0.1 T) and a high-frequency electromagnetic wave in the GHz range. When the microwave frequency matches the electron Larmor frequency the electron cyclotron resonance (ECR) mode is reached and the energy is deposited directly into the electrons in a well-defined volume. The design of the cavity is critical for microwave GIE to avoid reflection of the wave, which impacts the thrust level. Moreover, possible interferences with the spacecraft communication bands must be treated with care. Although less developed, ion engines in ECR mode at 2.45 GHz have been employed as the main propulsion system for the Hayabusa spacecraft [67, 68].

Whatever the ion thruster type, ions are extracted and accelerated to high velocity by means of a multi-aperture grid assembly [5, 6, 58]. The acceleration stage is commonly composed of two grids, as shown in figure 4. The first (screen) grid, which is in contact with the plasma, is set to a high electrical potential. It screens the electrons. The second (acceleration) grid is set to a low potential to accelerate ions. The exhaust velocity is directly given by the potential difference between the grids. The screen grid defines to a large extent the ion beam collimation. It also limits erosion of the acceleration grid by guiding the ion flux towards the output apertures. A third (deceleration) grid can be placed downstream of the second grid at a higher potential [6, 58], as shown in figure 5.

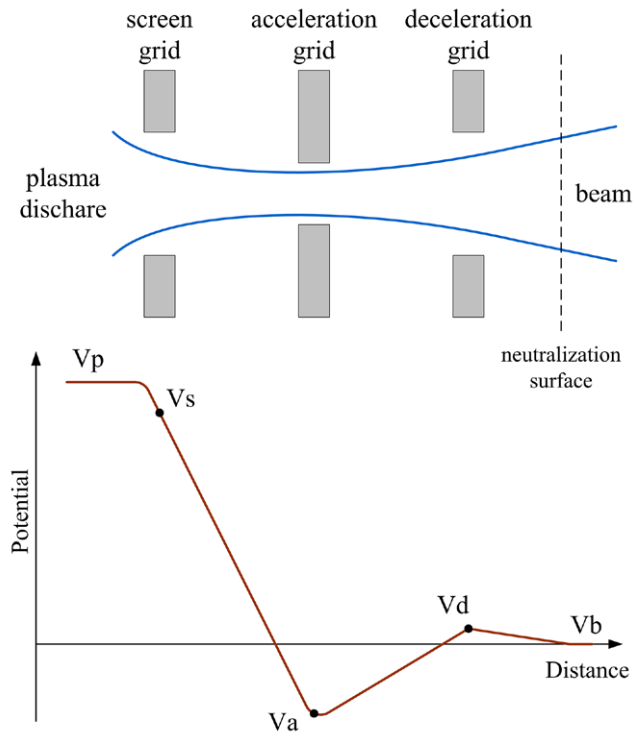

Figure 5. Schematic of a three-grid system in an ion engine with the corresponding potential profile along the aperture axis.

This third grid permits better separation of ion extraction and acceleration [6, 9], and in the end for a given beam power the net thrust is larger with a three-grid system. Even though the deceleration grid adds complexity and mass, it strongly reduces erosion of the acceleration grids by preventing cold charge-exchange ions produced near the exhaust from flowing back towards the thruster. In addition, it avoids the upstream migration of beam electrons. This unwanted side current decreases the efficiency and can damage the ion source. A four-grid ion thruster was successfully tested a few years ago [69]. Adding a fourth grid allows an increase in the maximum achievable ion kinetic energy, which is ≈10 kV with 2–3 grid ion optics due to electrical breakdown. Electrostatic neutralization of the extracted ion beam is realized downstream of the grid assembly where electrons from an external cathode, called the neutralizer, mix with the ions to form a quasi-neutral current-free beam [5, 6, 58]. The neutralizer is another critical component of a GIE. Its malfunctioning leads to a partial ion current neutralization and the resulting space-charge drastically decreases the thruster performance.

The thrust of an ion engine depends both on the velocity that is fixed by the potential drop between the grids and the ion mass flow rate. It is therefore related to the ion current flowing through the grid assembly. In order to increase the thrust level, the current has to be increased; there is nevertheless an upper limit [5, 6, 9]. The current entering the plasma sheath of a floating wall is the Bohm current $j_B = h\, n_0\, e\, v_B$, where h is the edge-to-bulk density ratio, n_0 is the bulk electron density and $v_B = \sqrt{kT_e/M}$ the Bohm velocity with k the Boltzmann constant. The h factor is 0.6 using the Boltzmann relation [70]; a more rigorous treatment can be found in [71]. The gap between the grids, which is filled solely with ions, forms a high-voltage sheath. In that case the ion current density j_i is limited by space-charge saturation and it obeys the Child–Langmuir law

$$j_i = \frac{4\varepsilon_0}{9}\left(\frac{2e}{M}\right)^{1/2}\frac{V^{3/2}}{d_{\text{eff}}^2}, \tag{15}$$

where V is the potential drop and d_{eff} the effective separation which is related to the grid spacing and accounts for the plasma meniscus [6]. The current density depends strongly on the potential and the grid separation. Small gaps are advantageous as higher voltages reflect in heavier power supplies. d_{eff} is typically 1 mm. With a 1 kV voltage, a value of $j_i = 15$ mA cm^{-2} is obtained for xenon. Using equation (15), the thrust per unit area of a GIE reads

$$\frac{T}{A} = \frac{8}{9}\varepsilon_0\left(\frac{V}{d_{\text{eff}}}\right)^2, \tag{16}$$

where A is the extraction area which accounts for the grid transparency. This equation shows that the thrust is proportional to the open area of the grids, i.e. to the size of the device, and independent of the nature of the propellant.

4.2. Performances and use

The electron density and temperature are typically $n_e \approx 10^{17}$ m^{-3} and $T_e = 2$–5 eV in ion engines. Standard performances are presented in table 3. As this technology produces a high specific impulse, often above the mission optimum, the thrust level is low, in compliance with equation (9). The thrust-to-power ratio is about 30–40 mN/kW and the thrust density is <10 N m^{-2}. Ion thrusters are heavy and bulky EP devices with a complicated power processing unit able to deliver high voltages and to manage various components. GIEs, however, offer several advantages. The thrust efficiency is above 70%. The high I_{sp} level readily translates into substantial propellant mass savings. The underlying physics is well understood and numerical simulations can perfectly predict performances and lifetime. The beam divergence angle is low (≈10 deg), hence interactions with the spacecraft components like solar panels are limited. The lifetime of a GIE is governed by the erosion of the grids under ion impacts. Extensive research on grid design and materials has demonstrated an operational life in excess of 30 000 h.

GIE technology has been exhaustively developed and tested. It is nowadays a very mature and well established technology. GIE can compete with other technologies for maneuvers like station-keeping and drag compensation. Their ability to operate efficiently at high I_{sp} makes them perfectly suited for energetic large Δv missions in which the time constraint is not critical [4, 72, 73]. They are the device of choice for unmanned deep-space exploration and journeys towards planets and asteroids. A list of recent space missions performed with GIE is given in table 4. In spite of their inherent low thrust level, electron bombardment ion engines have recently been used for transfer to the geosynchronous orbit of the first two all-electric communication satellites ABS-3A

Table 4. Solar system exploration missions based on electric propulsion.

Mission	Launch	Objective	Thruster	Sponsor
Deep Space 1	1998	Flyby of asteroid 9969 Braille and comet Borrelly	NSTAR ion engine	NASA
Hayabusa	2003	Asteroid sample return	ECR-type ion engine	JAXA
SMART 1	2003	Transfer to the moon	PPS1350 Hall thruster	ESA
DAWN	2007	Study of Vesta and Ceres protoplanets	NSTAR ion engine (evolution)	NASA
GOCE	2009	Earth gravity field measurement	T5 ion engine	ESA
Bepi Colombo	2017	Mission to Mercury	T6 ion engine	ESA

and Eutelsat 115. The selected ion engine (XIPS-702 from Boeing) nominally delivers 165 mN at 4.5 kW. The two satellites were launched in March 2015. They reached their final orbit in 6 and 7 months, respectively.

4.3. Annular geometry ion engine

A large research effort is presently ongoing in the United States to extend the performance capabilities of gridded ion engines [74]. The objective is primarily to maximize the thrust-to-power ratio to make GIE better adapted to orbit transfer applications. It is a question of exceeding the limitations on the achievable ion current density by improving the ion extraction capability as well as the source production. An appealing approach is the development of a non-conventional design: the annular geometry ion engine [75, 76] This design presents several advantages. The anode area for collecting electrons in the ionization chamber is increased compared to a conventional GIE of equivalent beam diameter. The engine is no longer source-limited, so it can operate at the current extraction limits of the ion optics. Consequently the thrust density is increased and an annular engine can operate at high power with moderate specific impulse. The annular design also enables the use of flat grids for extraction and acceleration, which improves efficiency compared to conventional spherically-domed circular grid assembly due to a high perveance. In addition, the flat electrode geometry of an annular engine simplifies the implementation, and pyrolytic graphite grids can be employed instead of carbon–carbon composites, which greatly improves the life capability. Pyrolitic graphite grids also offer a way of extending ion engine technology to very high power above 100 kW at reduced specific impulse (≈3000 s.)

5. The Hall thruster and variants

5.1. The HT

The HT is an electrical propulsion device for spacecraft that uses an electric discharge with magnetized electrons to ionize and accelerate a propellant gas. The original idea of ion acceleration in a quasi-neutral plasma was introduced in the mid-1960s and an HT was successfully operated in space for the first time in 1972 aboard the former USSR Meteor satellite [1, 77]. Since that time numerous experimental and theoretical works have been performed and the HT technology has equipped tens of commercial and military satellites. The main

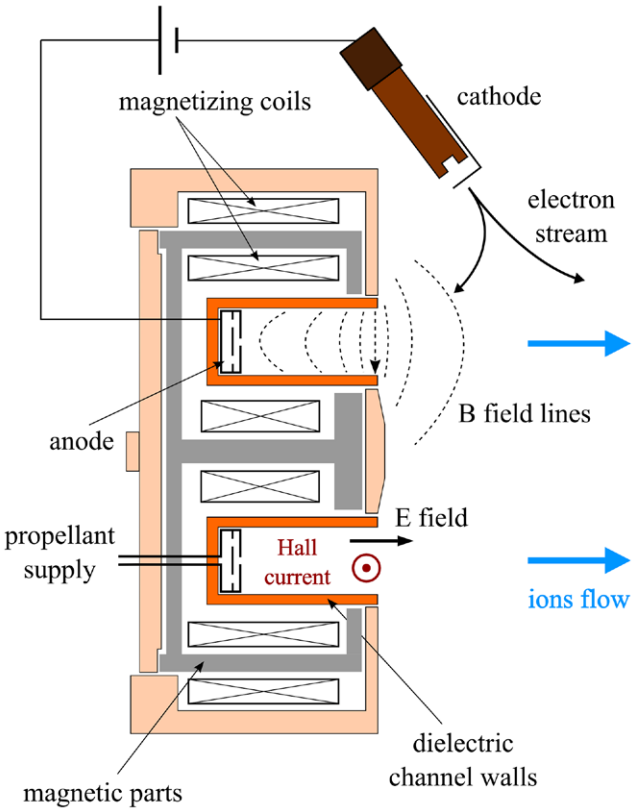

Figure 6. Schematic of a conventional annular HT with magnetizing coils and anode as fuel injector.

results of these works along with details about the HT physics, architecture and operation can be found in several books and reviews [6, 78–82].

Contrary to gridded ion engines, in an HT, the electrostatic acceleration of heavy atomic ions to high velocity occurs within the core of the discharge, which implies the use of a magnetized plasma able to sustain internal electric fields. A schematic of an HT is depicted in figure 6. The principle relies upon a magnetic barrier and a low-pressure DC discharge generated between a cathode and an anode in such a way that a crossed electric and magnetic field discharge is created [16, 78–80]. The anode is located at the upstream end of a coaxial annular dielectric channel that confines the discharge. The wall material is currently BN-SiO_2 [81]. The external cathode is a hollow cathode with an emissive element made of BaO or LaB_6 [6]. The emitted electron current corresponds to the discharge current I_d flowing in the electrical circuit. The largest part of the cathode current (≈80% I_d)

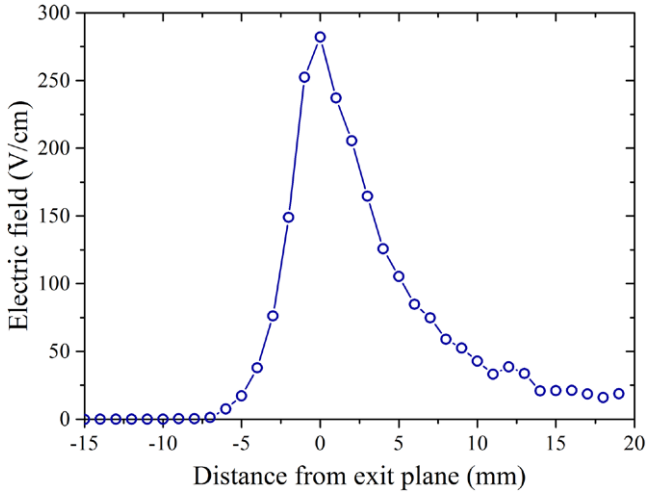

Figure 7. Electric field distribution along the channel axis of 1.5 kW Hall thruster obtained from laser-induced fluorescence measurements on metastable xenon ions [83] (300 V and 3 mg s^{-1}-Xe).

flows downstream to neutralize the ion beam. The remaining part travels towards the anode to maintain the plasma discharge. Electrons gain energy in the electric field, then they ionize the neutral atoms inside the channel. The propellant gas is introduced at the back of the channel either through the anode or using a dedicated injection system. In the latter case the anode and gas injector functions are disconnected, which facilitates management of the thermal load associated with the collected current. Magnetizing coils or permanent magnets, incorporated into a magnetic circuit made of iron or iron-cobalt alloys, provide a radially directed magnetic field **B** of which the strength is maximum in the vicinity of the channel exhaust. The magnetic field is chosen to be strong enough to make the electron Larmor radius much smaller than the discharge chamber characteristic dimensions, but weak enough not to affect ion trajectories: $B \approx 150$ G. The electric potential drop is mostly concentrated in the final section of the channel owing to the low axial mobility of electrons that are magnetically confined in this restricted area. Figure 7 shows the typical electric field distribution along the channel centerline of an HT. The magnitude of the axial component of the **E** field is ≈200 V cm^{-1} in modern devices that operate with applied voltages above 300 V. The field extends between the interior and the exterior of the channel; see [83] and references herein. The induced **E** field is a relevant quantity in an HT as it governs the propellant ionization and the ion acceleration, namely the thrust and the I_{sp}. The combination of the radial magnetic field with the axial electric field generates an $E \times B$ electron drift in the azimuthal direction. The drift current density, the so-called Hall current density, reads

$$\mathbf{j}_{e,drift} = -en_e\mathbf{v}_{e,drift} \quad \rightarrow \quad j_{e,drift} \approx en_e\frac{E_x}{B_y}. \quad (17)$$

The $E \times B$ current is the dominant conduction term in an HT as the operating pressure is low and the **B** field is weak. HTs are therefore often referred to as 'closed-electron-drift' thrusters. The electron density and temperature are typically $n_e \approx 5 \times 10^{17}$ m^{-3} and $T_e = 10$–50 eV in an HT firing with xenon. The high electron temperature explains the efficient ionization of the supplied gas. The propellant utilization α (see equation (7)) approaches unity. T_e also explains the large fractions of multiply charged ion species in the beam [6, 16], especially at high voltages. Their presence increases the I_{sp} but it reduces the thrust efficiency. Using the aforementioned values for the **E** and **B** field intensity, one finds $j_{e,drift} = 10.7$ A cm^{-2}. For a 1.5 kW-class device, the corresponding Hall current is ≈20 A whereas the discharge current reaches ≈5 A.

The standard performances are given in table 3. HTs provide a moderate specific impulse level (<2000 s) in contrast with GIEs, but the thrust-to-power ratio is 60 mN kW^{-1} and the thrust density is >30 N m^{-2} as there is no space-charge limitation on the ion current. The thrust efficiency is about 50%, but it is in excess of 60% for high-power thrusters. Losses have various origins in an HT [6, 16, 80, 84, 85], among others the large ion beam divergence angle (>30 deg), the production of highly charged ions, the charged-particle flux to the walls and the interrelation between ionization and acceleration processes [83]. The first three are linked to the large electron temperature. The thrust originates in the acceleration of the unmagnetized ions by the local electric field. The thrust generation has nonetheless an electromagnetic character as the result of the Lorentz force on the electron fluid: $\mathbf{j}_{e,drift} \times \mathbf{B}$. The HT is the only example of a hybrid electrostatic–electromagnetic plasma accelerator. HTs are technologically simple, compact and robust EP devices that offer interesting features in terms of thrust-to-power ratio, efficiency and mass. In addition, the associated power unit is more basic. They are therefore an attractive propulsion means for satellites. Low-power HTs (≈100 W) are well suited for drag compensation of observation satellites that operate on a low-altitude Earth orbit as well as for trajectory correction of microsatellite constellations. For many years 1 to 2 kW-class HTs have been employed for geosynchronous satellite attitude correction and station keeping. HTs with 5–10 kW normal power will soon be used for orbit transfer maneuvers of geosynchronous all-electric communication satellites following the successful Boeing experience with an ion engine. The selected thrusters are the XR-5 from Aerojet Rocketdyne, the SPT-140 from Fakel and the PPS®5000 from Snecma. Their large T-to-P ratio allows a shorter transfer duration compared to ion engines. HTs also appear to be good candidates for moving space probes, as demonstrated by the successful SMART-1 moon flyby solar-powered mission [86]; see table 4. The large thrust level makes high-power HTs (10–50 kW) suited for ambitious robotic missions like exploration of planets, moons, far-off comets and asteroids, as well as for transfer of cargo vehicles to support crewed missions. A good example is the forthcoming Asteroid Redirect Mission, whose spacecraft will use a set of 12.5 kW HTs [87].

5.2. Challenging issues

Despite several decades of HT development and investigation over a broad range of sizes and input powers, the physical mechanisms that govern the properties and the performance

of such a magnetized discharge remain poorly understood and poorly quantified. This lack of knowledge puts a brake on various aspects of the technology such as optimization of magnetic field topology, derivation of scaling laws, utilization of alternative propellants and development of predictive numerical models. A brief review of currently open questions is given hereunder.

5.2.1. Discharge oscillations. The crossed-field discharge of an HT is a highly non-stationary medium, which displays numerous types of plasma oscillations propagating either in an axial or azimuthal direction. These oscillations encompass many kinds of physical phenomena, each with its own length and time scales [80, 88]. Discharge fluctuations, of which the overall frequency range stretches from a few kHz up to several 100 MHz, play a major role in ionization, particle diffusion and acceleration processes. Longitudinal oscillations in the 10–30 kHz range, known as breathing oscillations, are especially of interest as they carry the majority of the power. Such oscillations find their origin in an ionization instability. They can merely be interpreted in terms of a prey–predator type mechanism between atoms and ions [89, 90]. Strong longitudinal oscillations are also observed in the 100–500 kHz range [91, 92]. These so-called ion transit time oscillations are triggered by high-frequency oscillation of the electric field in the acceleration region. Low-frequency oscillations (≈a few Hz) propagating azimuthally have been observed in the ionization layer of several HTs over a broad range of powers [93, 94]. These large-scale low mode number ($m = 1$ to 4) 'rotating spoke' instabilities are found in many $E \times B$ plasma devices. They probably originate in an ionization instability linked to the Alfvén critical ionization velocity. Their influence on electron transport and thruster performances remains unclear. Small-scale (in the order of the electron Larmor radius,≈1 mm) azimuthal oscillations with frequencies above 1 MHz have been detected experimentally and predicted by computer simulations [95–98]. These high-frequency high-wavenumber oscillations correspond to electron turbulence. They could play a dominant role in anomalous electron diffusion.

5.2.2. Electron transport. Although electrons are efficiently trapped in the magnetic barrier of an HT, a degree of diffusion towards the anode is necessary to guarantee current continuity. The classical formulation of the electron mobility perpendicular to magnetic field lines, which involves collision events with heavy particles, cannot, however, fully account for the magnitude of the electron current observed in the region of the large **B** field [99–101]. This anomalous electron diffusion can have two origins: near-wall conductivity or plasma turbulence. In near-wall conductivity, a primary magnetized electron is converted into a secondary electron, which, on the average, progresses one Larmor radius upstream [78, 102]. Evaluation of near-wall transport by means of numerical simulations indicates this mechanism is insufficient to explain the level of anomalous transverse electron diffusion [103, 104]. The turbulent cross-field diffusivity of electrons is of the Bohm type: it is due to stochastic fluctuations of the electric field azimuthal component and the electron density. When the fluctuations of E_θ and n_e are correlated in time in the presence of a radial magnetic field, electrons experience a net force in the axial direction responsible for transport towards the anode. Turbulent transport in the HT has long been attributed to instabilities; however, it is only very recently that clearer links between certain types of modes and electron transport have emerged. The small-scale high-frequency electron cyclotron drift instability, first identified in numerical simulations [97, 98, 105] and subsequently in experiments [95, 96] has been established as a candidate in causing anomalous transport. Experiments involving rotating spokes suggest that these large-scale structures may be responsible for carrying up to half of the current in the near-anode region [94]. A complete understanding of electron transport remains difficult to achieve. One reason is the complexity of the mechanisms which appear to be involved, as is evident from recent work showing that the electron cyclotron drift instability contributes to the electron current via both direct interaction with electrons and radial heating [106]. The relative contributions of, and interaction between, different instabilities have yet to be established, and may depend on features as diverse as the magnetic field topology and thruster operating conditions. The lack of accurate information regarding electron properties in the near-field region, inside the channel and in the vicinity of walls, increases the challenge of clarifying which mechanisms are at play.

5.2.3. Plasma-wall interactions. The interactions between the channel walls of an HT and the plasma have a drastic impact upon the discharge properties and the thruster performances and lifetime [81]. The degree of interaction is determined by the magnetic field topology and the nature of the wall material. The **B** field lines are perpendicular to the inner and outer channel walls, which leads to large charged-particle fluxes. Recombination and energy deposition at walls are therefore important [107, 108]. Walls are dielectric in HTs to avoid bypassing the magnetic barrier and to reduce heat transfer. The wall material is BN or BN-SiO_2, which enables high thrust efficiency and long operational life [81]. Dielectric materials nevertheless exhibit a large secondary electron emission (SEE) yield under the impact of electrons with energies between 10 and 50 eV. The conversion of plasma bulk hot electrons into cold electrons modifies the plasma sheath and the electron energy distribution function, with serious consequences on the thruster characteristics, through e.g. changes in the electron mobility and in the electric field profile. At high voltages, i.e. at high electron energy, the SEE from the wall can be so large that it compensates for the incoming electron flux. In that case, the sheath strength diminishes abruptly due to space charge saturation, which means the potential drop that usually repels electrons vanishes [102, 109–112]. The consequence is a large particle flux to the dielectric wall, hence a large energy transfer [108].

The lifetime of an HT is determined by the erosion of the channel walls under ion bombardment [113, 114]. Ions are accelerated towards the walls by the sheath potential drop and by the radial component of the electric field. The latter

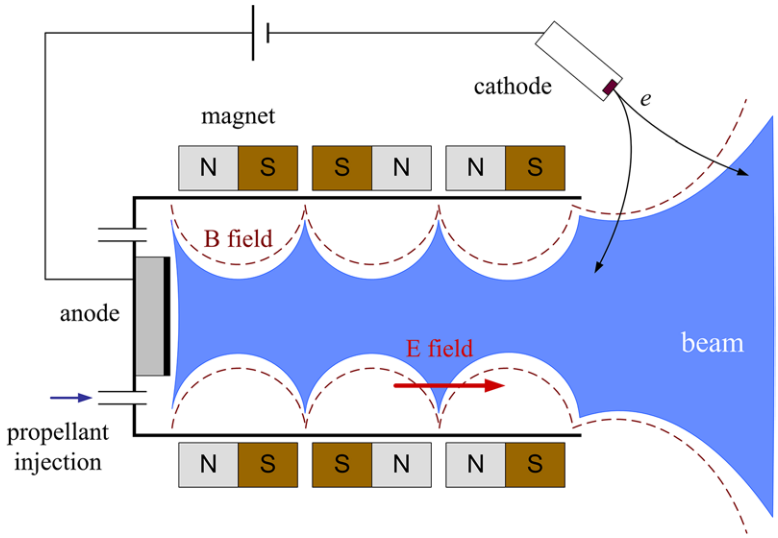

Figure 8. Schematic of a DC multistage cylindrical cusped-field thruster.

corresponds to the component parallel to the magnetic field lines. It is large due to the high T_e. The ion kinetic energy is then well above the sputtering threshold of the wall material. The thruster fails due to the loss of thermal or electrical insulation or when the circuit that controls the magnetic field topology is damaged. Anomalous erosion that creates ridges in the ceramic is also observed but the underlying mechanism stays ambiguous [78]. Modeling of the channel erosion is not yet reliable, mainly because data on the sputtering yield of ceramics at low energy are inaccurate. Predictive computer simulations would still avoid performing long and expensive lifetime tests.

5.3. Variations of the HT

Although the conventional HT architecture is the most common, there are variants that propose alternative options for specific aspects. The thruster with anode layer (TAL) offers a narrow acceleration region [80, 82, 115]: a guard ring at the cathode potential is placed at the channel entrance to better localize the electric field. This should increase the thrust efficiency and allow high I_{sp} operation by decreasing plasma–wall interactions. Up to now, the expected superiority of the TAL has not been demonstrated. Two-stage designs have also been proposed to improve the efficiency and to separate the ionization and acceleration regions. Prototypes with an intermediate electrode complexify the architecture and do not show any increases in performance [116–118]. Two-stage HTs using a microwave discharge to enhance ionization appear more promising [119]. Microwave discharge HTs deliver a larger thrust and a higher I_{sp} compared to single-stage thrusters with only a small decrease in thrust efficiency. Two-stage HTs remain an interesting option for propellants with a high ionization energy. Their development and optimization requires, however, a better understanding of the discharge physics.

The thrust efficiency and the lifetime deteriorate for small HTs operating at low power ($<$300 W) owing to a large surface-to-volume ratio [16]. Two approaches have been proposed for recovering good performances. Firstly, the channel width has been increased while keeping the mean diameter fixed [120]. The surface-to-volume ratio reduces and mirror effects increase. Experiments performed with a permanent magnet 200 W HT have shown the beneficial impact of a wide channel on the propellant utilization and thrust level [120]. The second approach is termed a cylindrical HT (CHT) [121–123]. Compared to an annular HT, the CHT has a lower surface-to-volume ratio due to a short annular region and a longer cylindrical region. The magnetic field topology differs in configuration: a CHT exhibits a cusp-type field distribution. The electron drifts are nevertheless closed and the CHT is an $E \times B$ propulsion device. The design of a CHT leads potentially to smaller wall losses. Below 200 W, CHT have performances similar to conventional HTs with a higher propellant utilization and larger fraction of multiply charged ions [124].

One possibility to enhance the plasma confinement in an HT is to use a cusped-type magnetic field configuration. The diverging cusped-field Hall thruster (DCHT) has been developed in the US [125–127] and the highly efficient multistage plasma thruster (HEMPT) has been built, tested and qualified in Germany [128, 129]. The primary motivation was to increase the lifetime while keeping the performances at a level similar to that of a standard HT. A schematic of a cusped-field thruster is shown in figure 8. The device is composed of a cylindrical or conical chamber with dielectric walls surrounded by magnets that create a cusped magnetic field configuration. The parallel magnetic lines along with the steep magnetic gradients (mirror effect) allow localization of the discharge away from the walls. The radial magnetic field lines at the cusp center create a magnetic barrier that reduces the electron mobility. The thrust efficiency of cusped-field thrusters seems correct. The HEMPT can operate at high I_{sp} with a high beam energy as ionization and acceleration processes are well separated. The propellant efficiency is rather low but this is compensated by the decrease in plasma–wall interactions. In addition, erosion of the discharge channel is seemingly negligible. The HEMPT appears to be a potential alternative to conventional HT, although the T-to-P ratio is lower and the divergence is larger. Moreover, the lifetime must be critically assessed.

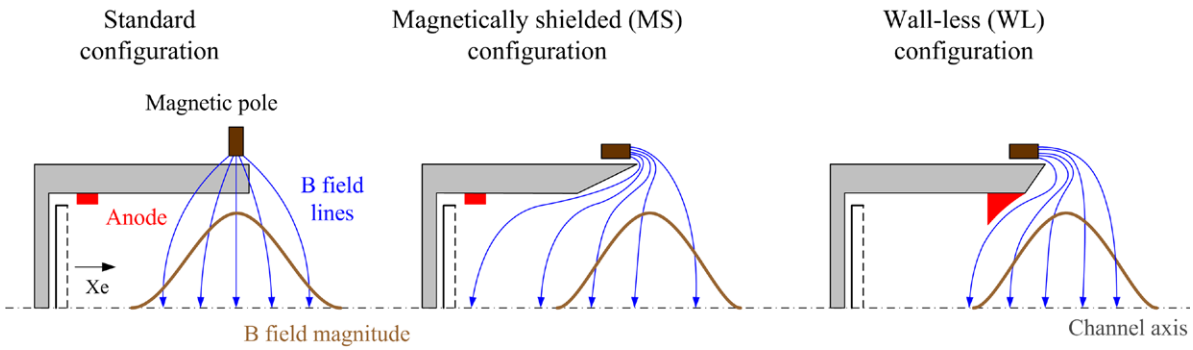

Figure 9. (Left) Basic configuration of a Hall thruster: the magnetic field lines intercept the walls. (Center) Magnetically shielded configuration: lines are parallel to the walls and they extend down to the anode. (Right) Wall-less configuration: the magnetic field lines are parallel to the anode that is placed at the exit plane.

One way of reaching a high thrust level involves clustering several HTs [130, 131]. Another, more effective and promising method is to combine HTs of various sizes and power levels to form a multichannel thruster, also termed a nested-channel HT [132, 133]. Nesting discharge channels reduces the thruster mass and size of a high-power system. Additionally, the nested-channel configuration broadens the operating envelope and facilitates throttling through the selection of available channels. To date, the nested channel technology has been successfully tested with two and three channels and it yields thrusters able to operate at over 100 kW of power.

6. Advanced EP concepts

6.1. HT in magnetic shielding and wall-less configurations

The main drawback of conventional HTs is the fact that the wall material determines to a large extent, through the secondary electron emission, the discharge properties, and consequently, the performance level as well as the operational lifetime, as discussed in section 5.2. The erosion of the annular channel walls in the acceleration region is due to bombardment by high-energy ions. Erosion occurs when the ion kinetic energy is above the sputtering threshold of the dielectric compound. Since ions acquire their energy in the plasma bulk and in the sheath, the magnetic field topology has an important impact on the erosion rate. The typical magnetic field line configuration of a conventional HT is illustrated in figure 9. In this configuration the magnetic lines form an efficient barrier and they intersect the walls. The electron temperature T_e is large both in the center and close to the walls: electrons move freely along a line and the medium is almost collisionless. Consequently, the large radial electric field component, which is parallel to the **B** field lines, and the large sheath potential drives a flux of high-energy ions towards the walls leading to erosion of the material, which drastically limits the HT lifetime.

An original approach to significantly reducing the erosion rate, hence prolonging the thruster lifetime, has been proposed and validated recently. This approach is termed magnetic shielding (MS) [134–138]. MS consists of preventing the magnetic field lines from crossing the walls in the acceleration region. Instead, the lines remain parallel to the wall of the downstream section of the channel and they extend deep into the channel, as shown in figure 9. The sheath potential fall at walls is reduced owing to the low T_e. The magnetic field lines that go along the corner of the beveled final section of the channel extend down to the anode where they capture cold electrons, hence a lower T_e in the wall regions. In addition, the MS topology strongly reduces the magnitude of the radial electric field component near the wall, and ion acceleration occurs away from the walls. Therefore an MS configuration allows a strong decrease in the wall material sputtering. The MS configuration has been successfully tested over a broad range of powers, from 300 W up to 20 kW. The wall erosion is effectively eliminated and the lifetime could certainly be extended by orders of magnitude. A high-power MS HT has been operated at high voltages for many tens of hours, delivering an I_{sp} of around 3000 s [139]. An MS HT has also been fired with conducting channel walls made of graphite [140]. Thrust and efficiencies stayed unchanged compared to BN walls, which confirms the efficient shielding effect of the topology. The weak point of an MS HT is the erosion of the magnetic poles, but this issue can be mitigated by using screens. In view of the remarkable improvements it brings, the MS configuration is the selected option for the 12.5 kW HTs of the Asteroid Redirect Mission spacecraft [87].

Another, more drastic, alternative has been proposed to limit interaction between the plasma and the surface in an HT. The principle is to shift the ionization and acceleration regions outside the cavity. This unconventional design is named a wall-less HT (WLHT) [141, 142]. In a WLHT, the anode is moved to the exit plane of the dielectric channel. The electric field is then entirely shifted outside the cavity, in a region where the magnetic field gradient is negative [141]. Although testing of the first prototype has demonstrated that the magnetized discharge can be moved outside the cavity without significantly compromising the ion production and acceleration, it also revealed deterioration of the performance [141]. The WLHT design can nevertheless be optimized by adapting the anode geometry and the magnetic topology in order to achieve performances close to the ones of conventional annular HTs. The strategy consists of avoiding the intersection between the anode and the magnetic field flux lines in order to prevent short-circuiting the magnetic barrier, as illustrated

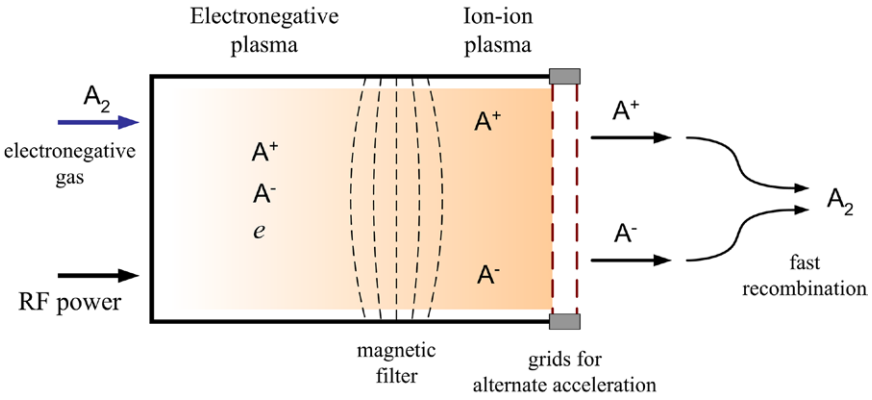

Figure 10. Schematic of the PEGASES negative ion thruster showing the main elements: the magnetic filter and the grid assembly for alternate ion acceleration.

in figure 9. As shown in recent experiments carried out with the 1.5 kW-class PPS-Flex HT, shaping the anode and adjusting the magnetic topology in parallel allows a strong reduction in the discharge current, an increase in the propellant utilization, and satisfactory thrust level, specific impulse and anode efficiency [142]. The WLHT is an interesting configuration mainly for two reasons: the mass and the volume can be reduced as the channel can be shortened and the magnetic topology is simpler in comparison with the MS approach. However, the lifetime must be critically assessed and efficient operation at high power and high I_{sp} has to be confirmed before considering the WLHT as a possible option for satellite propulsion and exploration missions.

6.2. Negative ion thrusters

The low mass of electrons makes them inefficient in producing momentum. As a consequence, all EP technologies call upon ions to generate thrust. But replacing electrons by negative ions, thereby maintaining the required plasma quasi-neutrality, offers new possibilities in the field of spacecraft propulsion. Negative ion thrusters have to make use of strongly electronegative molecules as a propellant, i.e. molecules with a high electron affinity that are able to easily produce negative ions by electron attachment. The basic principle of a negative ion thruster rests upon the creation of a stratified plasma with two distinct regions: a highly ionized plasma where negative ions are created followed by an electron free plasma, or ion–ion plasma, upstream of the acceleration zone, in such a way that both positive and negative ions provide thrust. A negative ion thruster would offer two advantages over conventional GIEs and HTs. Firstly, as both positive and negative ions are expelled, space charge neutralization is not needed. The device is therefore cathodeless, which increases the reliability level. Secondly, the downstream recombination of positive and negative ion pairs to form a neutral molecule is relatively fast, which guarantees a low charged-particle density in the beam. Consequently, interactions between the charged particles and the spacecraft elements like solar panels would be greatly reduced.

Until now, the only example of a negative ion thruster is the PEGASES concept. PEGASES is an acronym for plasma propulsion with electronegative gases. It is an unconventional RF gridded ion engine for which the discharge is created in a strongly electronegative gas [143, 144]. A layout of the PEGASES architecture and principle is outlined in figure 10. The ionization stage of PEGASES is divided into two main parts. In the first section, an inductively coupled RF discharge is produced with an electronegative gas such as sulfur hexafluoride (SF_6) or di-iodine (I_2) in a rectangular dielectric cavity. An electronegative plasma that contains electrons as well as positive and negative ions therefore fills the back of the cavity. In the second section, the electronegative plasma is transformed into an ion–ion plasma through a magnetic filter [145]. Electrons are trapped in the region of the strong magnetic field. Due to collisions with neutral heavy particles, the electron temperature quickly drops. Subsequently, cold electrons attach to molecules to form negative ions. Afterwards, the ion–ion plasma is electrostatically accelerated through an assembly of two polarized grids. An extraction scheme based on an alternate positive and negative grid voltage is validated when an electron-free plasma state is reached [146–148]. Positive and negative ions are extracted and accelerated periodically in such a way that downstream beam neutralization is continuously maintained. The screen grid is polarized with a square-wave voltage, while the acceleration grid is grounded. Efficient extraction and beam neutralization are achieved when the modulation frequency approaches the ion plasma frequency. The PEGASES prototype performances have been assessed from measurements of ion fluxes and ion energy [144]. The performances are low at this stage but they can certainly be improved by optimizing the magnetic filter, the geometry and the ion optics. The main disadvantage certainly arises from the associated power unit, which would be complex and heavy. Even though the working principles of the PEGASES thruster have been demonstrated, several points are still to be studied before PEGASES can compete with established technologies. The space charge compensation in the beam must be verified in a low-pressure environment with no secondary plasma. The thrust, beam divergence and efficiencies have to be experimentally determined. Moreover, an important matter to clarify is the impact of the corrosive nature of the gaseous electronegative propellant on the life capability of the device.

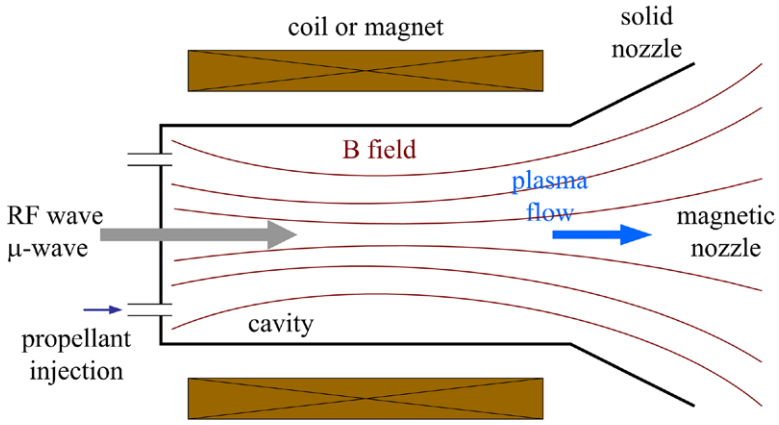

Figure 11. Outline of an electrodeless plasma thruster. The power is transferred to the gas from microwaves or RF waves. The plasma expands through either a solid nozzle or a magnetic nozzle. No neutralizer is required.

6.3. Electrodeless plasma thrusters and the magnetic nozzle

All EP technologies described in the preceding sections, with the exception of the low-I_{sp} resistojet, employ electrodes exposed to the plasma to produce and/or accelerate the current at the origin of the thrust. Electrodes, however, wear out and erode over time, especially at high power levels, which restrains the thruster lifetime and decreases the reliability. Over the past two decades, various approaches and architectures that avoid using exposed electrodes have been developed and successfully tested; see e.g. [9, 10, 12] and references herein. Figure 11 shows a schematic drawing illustrating the general principle of an electrodeless electric thruster. The power is deposited into a gaseous propellant by means of microwaves or RF waves. The wave can be coupled to a magnetic field produced by either coils or magnets in order to improve electron or ion heating and ionization. The plasma is generated in a cylindrical dielectric chamber. It expands into the vacuum through a solid nozzle or a magnetic nozzle where thermal energy is converted into direct kinetic energy. Electrodeless thrusters therefore fit into the electrothermal accelerator category. According to both the ionization degree and the electron temperature, the thrust originates either from the expansion of a hot gas or from acceleration of ions. The latter mode is preferred as efficiencies are higher. Electrodeless plasma thrusters do not require an external neutralizer as a quasi-neutral plasma is expelled out of the chamber: additionally they are cathodeless.

Before describing different electrodeless thruster concepts, it is interesting to give an idea of the expected thrust level of such devices [9]. We consider a homogeneous xenon plasma at 0.2 Pa with the following parameters: $n_e = 10^{18}\,\mathrm{m}^{-3}$, $T_e = 4$ eV and $V_p = 20$ V. Such values can be achieved with e.g. 200 W of RF power in inductively coupled mode. The entire plasma expands from a 5 cm in radius R glass tube into a perfect vacuum. When applying a treatment similar to that of a wall sheath, the thrust delivered by the Xe^+ ion flow reads

$$T = \dot{m}_i v_i = \pi R^2 M n_e v_B v_i = \pi R^2 M n_e \sqrt{\frac{k_B T_e}{M}} \sqrt{\frac{2eV_p}{M}}. \quad (18)$$

The plasma potential at infinity is assumed to be zero. The thrust reaches 16 mN and the I_{sp} is about 550 s. The thrust obtained from the neutral gas expansion is comparatively low: with a gas temperature of 350 K, the thrust is ≈1.5 mN. Performances of real devices are of course lower due to loss terms and gradients. This quick analysis, however, indicates that T_e and V_p must be high, which means the source must operate at low pressure to achieve good performances.

6.3.1. RF plasma thrusters. RF plasma thrusters differ according to the coupling mode of the RF discharge: capacitive mode, inductive mode and wave (helicon) mode when a static magnetic field is applied [149]. As the mode is connected to the plasma density, it also defines the way thrust is generated. For capacitive plasmas, the thrust is due to the neutrals. In inductive and helicon modes, the ion contribution largely prevails over the neutral contribution.

In the so-called RF plasma thruster, the energy source of the device is a high-pressure (≈100 Pa) capacitively coupled RF discharge [150, 151]. The thrust is then produced by the expansion of a hot neutral gas as the ionization degree is low [12], like in resistojets and arjects. Neutral gas heating mostly results from ion-neutral collision events, i.e. charge-exchange and elastic collisions, as well as from heating at the plasma cavity walls [152, 153]. A nozzle can be added to the cylindrical cavity to enhance performances. RF plasma thruster concepts can potentially provide thrust in the milli-Newton range when operating at around 100 W with a specific impulse of several tens of seconds. The RF plasma thruster meets stringent power, size and mass limitations of microsatellite propulsion systems while achieving specific impulse comparable to larger chemical engines. However, it competes with low-power resistojet devices that operate in DC mode with good efficiencies.

The helicon thruster is a relatively new and promising electrodeless and cathodeless device for space propulsion based on a low-pressure high-density RF helicon source in which the thrust arises from the acceleration of ions [9, 10, 12]. The thruster is composed of a dielectric (quartz) tube surrounded by magnetizing coils or magnets that produce an axially directed magnetic field of 100–500 G. The axial **B** field permits the launch, the propagation and the absorption of helicon waves. It also reduces the plasma diffusion towards

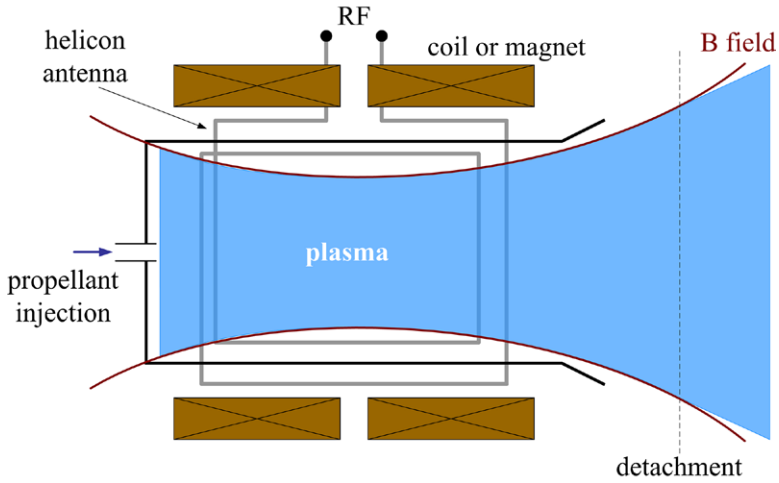

Figure 12. Schematic of a helicon plasma thruster.

the cavity walls, which tends to increase the plasma density. In addition, the magnetic field lines diverge outside the tube (see figure 12), which creates a magnetic nozzle to guide and accelerate the plasma. A RF antenna, which typically operates at between 1 and 30 MHz, is wrapped around the tube to transfer the power in inductive or helicon mode. Helicon waves are low-frequency ($\omega \ll \omega_{pe}$, where ω_{pe} is the plasma pulsation) electromagnetic waves that propagate in magnetized plasma. The wave rotates during its propagation in the **B** field direction, making the electron motion helical, hence the term *helicon* [149, 154, 155]. In helicon discharges, the energy is directly transferred from the wave to the electron population, which, through collisional and collisionless heating mechanisms, leads to a high ionization degree in large plasma volumes. The helicon wave propagation depends on n_e for a fixed magnetic field amplitude; i.e. in some regions of the plasma or of the jet the coupling is inductive. Helicon sources provide efficient wave heating and plasma confinement, so they create relatively high plasma densities ($n_e > 10^{17}$ m^{-3}) at low input powers (hundreds of watts). Furthermore, they can operate under a broad range of parameters like gas flow rate, power, frequency and magnetic field.

A fraction of the energy transferred to the electrons serves to ionize the gas; the other part is converted into ion kinetic energy in the magnetic nozzle. Therefore a high electron temperature is necessary to achieve large I_{sp} values and high thrust efficiencies. In certain circumstances, e.g. a diverging **B** field, a non-neutral current-free double-layer (DL) may form within the plasma. A DL is in a way similar to a collisionless electrostatic shock front [9, 156, 157]. Ions are then accelerated throughout the potential drop that exists in the DL. Observation of a fast ion beam emerging from the DL led to a new type of plasma thruster, referred to as the helicon double-layer thruster or HDLT in short [158–161]. But as shown later, the DL does not contribute to thrust generation as the total momentum stays constant in a DL [162, 163]. The DL, however, allows the formation of a large-area collimated plasma beam, which improves performances. Functionality of the HDLT concept has been demonstrated for a variety of propellants, powers, magnetic fields and geometries. Direct thrust measurements have also been performed to evaluate the HDLT capabilities with krypton and argon [164–166]. The thrust level is low, typically ≈1 mN for 100 W of RF power, and the propulsive thrust efficiency is ≈1%. The specific impulse stays below 500 m s^{-1}. These poor performances result from a low propellant utilization and a weak ion acceleration. Testing has been performed recently up to 2 kW with argon as a propellant, and improvements were noted [167, 168]. The measured thrust was in excess of 10 mN. The specific impulse reached several hundreds of seconds. The maximum thrust efficiency was 7%, which clearly relates performances to size and power. Helicon thrusters remain at an early stage of development. A better understanding of the underlying physical mechanisms along with further system optimization are required for the helicon thruster to become a viable alternative to conventional EP technologies.

6.3.2. Microwave plasma thrusters. Instead of RF waves, high-frequency microwaves can also be used to produce and to energize the plasma in electrodeless thrusters [169]. Even though the concept of a μ-wave plasma engine was first investigated in the 1960s, there is nowadays a renewed interest in this technology, certainly motivated by potential needs of the EP market. One of the most advanced concepts is the low-power coaxial plasma thruster that relies on the ECR configuration to efficiently transfer the energy of the wave to the plasma [170, 171]. The originality of this device is its coaxial geometry that allows a strong reduction in size compared to typical waveguide ECR sources, and operation at low input power. A schematic of the coaxial ECR thruster is shown in figure 13. A coaxial guide is connected to an aluminum cylinder 13 mm in outer diameter and 15 mm in length. The conducting core is a stainless-steel rod 2 mm in diameter and ≈15 mm in length. The electric field generated by the μ-wave is purely radial inside the cavity. A dielectric plate, through which the gas is injected, insulates the back of the cavity. A set of permanent magnets or magnetizing coils surround the cavity. They provide an axially directed magnetic field with maximum amplitude around 900 G in the rear section of the cavity. The magnetic field plays three roles.

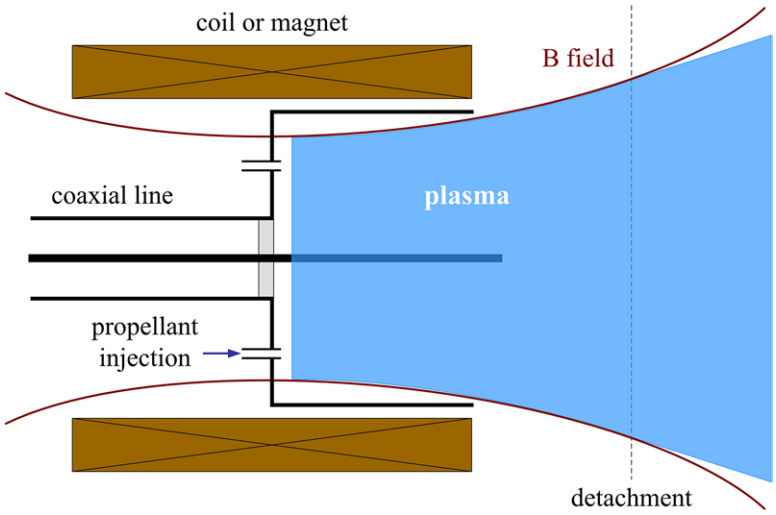

Figure 13. Schematic of the coaxial ECR plasma thruster [173].

Firstly, it allows ECR heating of the electron fluid. Secondly, it confines the plasma by limiting diffusion towards the walls. Thirdly, the **B** field lines form a diverging magnetic nozzle downstream of the cavity exit plane, which accelerates ions, therefore producing thrust and I_{sp}.

The microwave power at 2.45 GHz is efficiently transferred to the plasma via the ECR mechanism [70]. The resonant absorption occurs when the frequency of the microwave electric field ω_μ matches the cyclotron frequency ω_{ce} of the magnetized electrons. Microwave energy is absorbed via a collisionless process in the narrow resonance region. Inelastic collisions between hot electrons and neutrals subsequently lead to an efficient ionization of the gas as a whole. ECR sources achieve both a high-plasma density ($n_e \approx 10^{18}$ m^{-3}) and a high electron temperature ($T_e \gg 10$ eV) at a power level of a few tens of W. Recent works on the coaxial ECR thruster indicate an ion kinetic energy around 400 eV and an electron temperature in the source above 60 eV with only 50 W of microwave power [172, 173]. Such numbers are remarkable for a low-power thruster. Naturally, the highest efficiency is observed at low pressure, i.e. at low mass flow rate, when T_e is the largest. Performances of the coaxial thruster have been assessed with Ar and Xe as propellants by measuring the ion current as well as the ion energy in the jet [172, 173]. Best performances are achieved with xenon: 1 mN of thrust, 1000 s of I_{sp} and a total efficiency of 16% for a power of 30 W. The thrust-to-power ratio is then 33 mN kW^{-1}, which is comparable to what a gridded ion engine delivers.

Like the helicon thruster, the coaxial ECR thruster is simple, compact and electrodeless, it does not require a neutralizer and it can operate with a wide variety of propellants. Nevertheless the coaxial ECR thruster seems more efficient at low power with a much higher specific impulse. Although further research is needed, e.g. on the coupling between wave and plasma and on the design optimization, and although the thrust has to be directly measured, the technology is promising and it could certainly find applications on board small satellites and for some missions requiring long operational lifetimes.

6.3.3. VASIMR. The concept of the MW-class VASIMR engine, an acronym for Variable Specific Impulse Magneto Rocket, emerged in the 1980s. However, the standard architecture based on a helicon plasma source was only suggested in the mid-1990s [174–176]. The VASIMR is a massive and complicated propulsion system composed of three stages arranged one after the other. Firstly, a RF helicon plasma source is used to create a high-density plasma. An ion cyclotron heating (ICH) stage is used next to further energize the plasma in order to reach a very high ion temperature. RF waves in the frequency range of 1–100 MHz are used for both cyclotron magnetic resonance heating of ions and non-resonant heating of electrons. ICH requires ions to be magnetized, which implies the generation of a strong magnetic field. The VASIMR engine is then equipped with large superconducting magnets able to generate a 2 T magnetic field strength. The last stage consists of an applied expanding magnetic field that creates a magnetic nozzle where thrust is produced. The nozzle efficiently converts perpendicular ion kinetic energy into directed parallel ion kinetic energy through conservation of the magnetic moment and conservation of the ion kinetic energy. Additional ion velocity can also result from the transfer of the electron thermal energy into ion kinetic energy by means of weak ambipolar electric fields in the magnetic nozzle. Notice that the magnetic nozzle is surrounded by a solid nozzle through which neutral gas can be injected to increase the thrust level. The neutral gas is dragged along and accelerates by collision events with fast moving ions. VASIMR has been operated with hydrogen and helium as the propellant gas in the past. Argon and krypton are nowadays the usual propellant.

The most advanced version of VASIMR is the VX-200 prototype designed to operate at 200 kW of input DC electrical power. The performances of the VX-200 engine have been measured with argon and krypton to evaluate the status of the technology [177, 178]. The VX-200 was able to generate 6 N of thrust and to produce a specific impulse of about 5000 s at 200 kW of total power with the helicon and ICR stages operating together. The thrust efficiency was 70%. Those numbers

can be compared with performances of MPD thrusters, which are high-power devices too; see section 3.2. The Li-LFA MPD thruster delivers a higher thrust and a similar I_{sp} at 200 kW. The efficiency is lower,≈50%. The two technologies could compete as high-power EP devices for orbit transfer of heavy payloads, for cargo missions to the moon and near Earth asteroids, and for reducing the trip time of robotic and interplanetary missions. Although much progress have been achieved during the past years, the VASIMR engine must still demonstrate reliable and efficient operation during long time periods. Moreover, complexity, heat load management and mass of the system are technical obstacles that have yet to be overcome.

6.3.4. Principle of a magnetic nozzle. The three plasma thruster concepts previously described, along with the AF-MPD engine, employ as an acceleration stage an expanding magnetic field that forms a divergent magnetic nozzle [10, 179–181]. The purpose of a magnetic nozzle is to transform the internal energy of the plasma into axially-directed ion kinetic energy. The plasma is then accelerated supersonically into the vacuum. In essence the purpose of a magnetic nozzle is similar to that of a traditional solid de Laval nozzle. There are, nevertheless, several differences in their basic principle. A magnetic nozzle has no physical boundaries and it guides and confines charged particles: losses are reduced and the lifetime issue is avoided. The mechanisms at the origin of the plasma acceleration and thrust generation, including plasma detachment, are much more complicated in the case of a magnetic nozzle due to the presence of long-range electric and magnetic forces and because the physics at play depend on the way the internal plasma energy is stored.

As a first approximation, the functioning of a magnetic nozzle relies upon the force exerted on a charged particles along a magnetic field line. In the case of a stationary **B** field and under the adiabaticity hypothesis, i.e. variations of **B** are small with respect to the Larmor gyration radius and the cyclotron frequency, the force parallel to a magnetic stream line reads [70]

$$\mathbf{F}_{\parallel} = m\frac{\mathrm{d}\mathbf{v}_{\parallel}}{\mathrm{d}t} = -\mu\nabla\mathbf{B}_{\parallel}, \tag{19}$$

where μ is the magnetic moment of the particle: $\mu = E_{\perp}/B_{\parallel}$, where $E_{\perp}$ is the particle kinetic energy perpendicular to the field line. The magnetic moment is an adiabatic invariant, which means it is conserved in the course of the motion. When $B_{\parallel}$ increases, $E_{\perp}$ increases as well to keep μ constant. As the energy is conserved, the particle velocity along the field line rises in collisionless media. As a consequence, the force $F_{\parallel}$, which is independent of charge, pushes the particle into regions of smaller magnetic field. $F_{\parallel}$ is therefore responsible for the acceleration of charged particles in a diverging magnetic nozzle with decreasing magnetic strength. We shall only consider here the case where only the electrons of the plasma are magnetized, i.e. their Larmor radius is low and their Hall parameter is large (no collisions). The case with a fully magnetized plasma, which corresponds to the VASIMR engine, is somewhat more difficult to treat. In the magnetic nozzle, strongly magnetized electrons move downstream due to $F_{\parallel}$ and they tend to follow the magnetic stream lines. On the contrary, massive unmagnetized ions tend to escape the magnetic nozzle. In order to warrant the plasma quasi-neutrality, ambipolar electric fields develop perpendicular to the magnetic field lines [182–184]. In addition to maintaining the plasma cohesion, the ambipolar electric fields allow the conversion of the electron thermal (perpendicular) energy into directed ion kinetic energy. In short, the ions are accelerated in the ambipolar potential drop, the latter being controlled by the electron temperature in the source and the electron cooling rate throughout the nozzle.

A final aspect of a magnetic nozzle is the detachment of the plasma from the magnetic field lines: after a full expansion, the plasma must detach to continue flowing freely [185]. This phenomenon is critical for magnetic nozzle efficiency. If the plasma does not detach, there is no net momentum production. If the plasma detaches too early, full energy conversion is not achieved and efficiency is low. Conversely, if the plasma detaches too late, the divergence is high and the thrust is low. There is clear experimental evidence, e.g. thrust production, that the plasma detaches from the magnetic nozzle of the electric thrusters. Nevertheless, the underlying physical mechanisms are not yet well understood and magnetic nozzle physics are an active field of research. One possible detachment process is the diffusion of electrons, owing to either collisions with heavy particles (resistivity) or electron inertia, which is especially applicable to high-energy electrons [185]. Another possibility is the change in magnetic field topology due to the induced field [176]. A final option is the ion or electron demagnetization [186].

7. Propellant options

One of the important elements of an EP system is obviously the propellant. This determines to a large extent the thrust efficiency and the level of specific impulse. In addition, nature, storage feasibility, flow control and injection of the propellant have a major impact on the complexity and the overall cost of a spacecraft propulsion assembly as a whole. Selection of the right propellant is therefore a critical step in the development of an EP system. Xenon is currently the propellant of choice for various electric thrusters, including HTs and ion engines, whatever the spacecraft type, i.e. satellites versus exploration probes. Although xenon has several advantages, it also has many disadvantages that might force the community to consider alternative propellant options as both the number of available technologies and the diversity of vehicles, missions and maneuvers are growing.

Many factors and practical issues contribute to the suitability of a propellant for EP [187–191]. Some physical properties of various propellants, including xenon as a point of reference, are given in table 5, along with the toxicity level and the cost range. Factors that affect the performances are the mass and the ionization energy. A heavy propellant delivers more momentum but at the expense of the specific impulse. A suitable propellant combines a low ionization threshold with a high ionization cross-section to minimize the amount of

Table 5. Properties of various propellants for electric propulsion.

Propellant	Mass (amu)	E_i (eV)	State	Vapor pressure (Pa)	Melting/boiling point (°C)	Toxicity	Cost
He	4.0	24.6	Gaseous	—	−272 /−269	Low	Low
Li	6.9	5.4	Solid	10^{-6} (500 K)	180 / 1342	Medium	Low
Ar	39.9	15.8	Gaseous	—	−189 /−186	Low	Low
Kr	83.9	14.0	Gaseous	—	−157 /−153	Low	High
Xe	131.3	12.1	Gaseous	—	−112 /−108	Low	Very high
Cs	1.2.9	3.9	Liquid	3×10^{-4} (300 K)	29 / 685	Low	Very high
Hg	200.6	10.4	Liquid	0.4 (300 K)	−39 / 357	High	Low
Bi	209.0	7.3	Solid	0.5 (900 K)	271 / 1564	Medium	Low
I_2 (I)	253.8 (126.9)	9.4 (10.4)	Solid	40 (300 K)	114 / 184	Medium	Low

Note: E_i refers to the first ionization energy. The dissociation energy of I_2 is 1.57 eV.

energy necessary to create a high-density plasma. Molecular propellants must generally be avoided as part of the available input power is lost into dissociation in smaller fragments and into excitation of internal vibration and rotation modes. The iodine molecule (I_2) might be an exception as it is attractive in many other ways. Some technical and practical aspects must also be accounted for when analyzing propellant options. The propellant must be easy to store in order to reduce the complexity of the tank and associated sub-systems without changes in the power processing unit. Liquid and solid propellants bring here an obvious benefit as gaseous atomic propellants like Xe and Kr are stored in the supercritical fluid state, which necessitates large high-pressure (200–300 bars) tanks. Condensable propellants, on the other hand, introduce specific requirements since the mass flow system and the gas feeding system are more complicated to operate. A liquid/solid compound with a high vapor pressure and with low melting and boiling temperatures is preferred, as any power that is used for evaporation and to maintain the temperature of the transfer line and injection system reduces the overall efficiency of the thruster assembly. For instance, iodine vapor can be created from solid I_2 and the mass flow rate can be thermally regulated with a relatively low temperature ($\leqslant$100 °C), which make the associated power very low [192]. For comparison a Bi feeding system operates at about 300 °C [194, 195]. Another relevant point is that the propellant must be non-radioactive (e.g. radon), non-toxic and easy to handle. Contamination may also be a critical issue for thruster elements as well as for spacecraft elements like solar arrays and radiators. Condensable propellants can deposit if the surface temperature is below their melting point. Coating formation leads to a change in the electrical and optical properties of the components. Propellants can also chemically react with various materials, which means a high level of cleanliness of the feeding system must be achieved, and compatibility with thruster and spacecraft materials must be ensured. This aspect is particularly important for I_2, which is strongly corrosive for many metals and alloys [193]. Availability and cost are additional relevant criteria. A low-cost option is better, especially for long-duration missions, which translates into a large amount of propellants. One last point must be considered, although it can be regarded as secondary. The propellant has an impact on ground testing. A low background pressure ($\approx10^{-6}$ mbar) is needed during testing to avoid artificially modifying thruster performances and beam characteristics. With gaseous propellants, a cryogenic pumping system with a very large pumping speed is employed to evacuate the chamber. Cryogenic systems are complex and expensive, especially for high-power devices [35]. Contrary to gaseous propellants, condensable propellants will naturally condensate on the chamber walls. Pumping can then be achieved by controlling the wall temperature. Nevertheless, there are contamination issues if the propellant is toxic or reactive.

According to the aforementioned list of criteria for propellant selection in the field of EP, there are three attractive candidates for an alternative to xenon. Krypton generates a high specific impulse and no significant modifications of the thruster assembly are required. It is also a non-toxic propellant. However, the thrust efficiency is lower due to a poor ionization degree and its storage density is below that of xenon. Bismuth is a low-cost propellant that offers a large thrust-to-power ratio due to its high mass and high ionization efficiency. In addition, its storage density is six times that of xenon. The main drawback arises from the fact that a high temperature is required to prevent condensation. The thrust efficiency achieved with iodine (I_2) is similar to that obtained with xenon. Although the ionization energy of I_2 is low and the cross-section large, energy is lost into dissociation and excitation and the average mass is close to the I atom mass. But an iodine-vapor feeding system can be operated at relatively low temperature. Moreover, the storage density of I_2 is three times higher compared to xenon and a high purity grade is relatively inexpensive. The disadvantage lies in the fact that iodine is a reactive compound and compatibility with the thruster and space vehicle must be guaranteed. In conclusion, one must keep in mind that there is no ideal propellant. The selection results from a trade-off between various criteria, evaluating pros and cons. Furthermore, the final choice also depends upon the spacecraft design and the mission objective and duration.

8. Summary and prospects

EP encompasses a large variety of technical solutions and devices which cover a broad range of sizes, powers, thrusts,

specific impulses and efficiencies. Some thrusters have a long flight heritage and are commercially available whereas others are currently prototypes under development and testing in laboratories. There is obviously no *ideal* or *perfect* electric thruster for space applications. The technology must be selected according to the spacecraft design, the budget, the propulsion requirements and the mission objectives. The primary advantage of EP systems is the propellant mass economy, especially for missions with a large velocity increment. Electric thrusters also offer secondary benefits like precision and variability of the thrust, restart capabilities and long total operational time. Their major disadvantages are the need for complicated external power sources and the low thrust density levels. This last characteristic strongly limits near-planet applications, complicates and elongates orbit transfers, and makes launch and ascent/descent maneuvers unfeasible. EP is in fact fully exploited in the domain of interplanetary trips. It even enables missions that simply could not be performed with chemical propulsion. Suited missions for EP include heavy cargo missions to the moon and Mars, journeys towards asteroids and giant outer planets and their moons, as well as sending unmanned probes beyond the solar system.

EP has been positively evaluated and successfully employed aboard many commercial and military satellites over the past decades. The interest in EP systems is nevertheless currently taking a step forward for two reasons: the appearance of all-electric communication satellites and the recognized benefit for small satellites, constellations and science probes. Without doubt the quantity and the variety of efficient EP systems will significantly increase in the near future. As regards ambitious EP-based space missions with large velocity increments, the situation is somewhat different. Although high-power high-thrust devices have already been developed and investigated as MPD thrusters, HTs and the VASIMR engine, several issues and challenges remain. The lifetime and the stability of the devices must be warranted for durations that greatly exceed what has been achieved in ground-test facilities so far. Answers rely on research activities dedicated to new materials, improved or modified architectures and plasma confinement. Another key concern is the energy source. Even though the efficiency of solar panels will certainly improve, nuclear energy remains the only possibility for deep space exploration. Therefore, compact high-power nuclear fission reactors will have to be deployed in space, which represents a technological challenge and a political challenge as well. It is, however, the price to be paid for pushing the frontiers of human knowledge.

Acknowledgments

The author wishes to thank his colleague Dr S Tsikata and his former PhD student Dr J Vaudolon for their always pertinent remarks and advice. Thanks also go to all the members of the ICARE EP team for accepting the limited time devoted to their work during the writing of this manuscript. Finally, the author warmly thanks colleague and friend Prof M Dudeck for reading the first version of this review, for his judicious comments and his support.

References

[1] Choueiri E Y 2004 A critical history of electric propulsion: the first 50 years (1906–56) *J. Propul. Power* **20** 193–203
[2] Sutton G P and Biblarz O 2010 *Rocket Propulsion Elements* (New York: Wiley)
[3] Turner M J L 2009 *Rocket and Spacecraft Propulsion* (Chichester: Spinger)
[4] Frisbee R H 2003 Advanced space propulsion for the 21st century *J. Propul. Power* **19** 1129–54
[5] Jahn R G 1968 *Physics of Electric Propulsion* (New York: McGraw-Hill)
[6] Goebel D M and Katz I 2008 *Fundamentals of Electric Propulsion* (Hoboken, NJ: Wiley)
[7] Jahn R G and Choueiri Y 2002 Electric propulsion *Encyclopedia of Physical Science and Technology* vol 5, 3rd edn (San Diego: Academic) pp 125–41
[8] Martínez-Sánchez M and Pollard J E 1998 Spacecraft electric propulsion—an overview *J. Propul. Power* **14** 688–99
[9] Charles C 2009 Plasmas for spacecraft propulsion *J. Phys. D: Appl. Phys.* **42** 163001
[10] Ahedo E 2011 Plasmas for space propulsion *Plasma Phys. Control. Fusion* **53** 124037
[11] Garrigues L and Coche P 2011 Electric propulsion: comparison between different concepts *Plasma Phys. Control. Fusion* **53** 124011
[12] Charles C, Boswell R W and Takahashi K 2012 Investigation of radiofrequency plasma sources for space travel *Plasma Phys. Control. Fusion* **54** 124021
[13] Armano M *et al* 2015 The LISA Pathfinder mission *J. Phys.: Conf. Ser.* **610** 012005
[14] Frisbee R H 2009 Limits of interstellar flight technology *Frontiers of Propulsion Science* (*Progress in Astronautics and Aeronautics* vol 227) ed M G Millis and E W Davis (Reston, VA: AIAA) pp 31–126
[15] Gibson M A, Mason L S, Bowman C L, Poston D I, McClure P R, Creasy J and Robinson C 2014 Development of NASA's small fission power system for science and human exploration *Proc. of the 12th Int. Energy Conversion Engineering Conf.* (Cleveland, OH: AIAA) paper 2014–3458
[16] Dannenmayer K and Mazouffre S 2011 Elementary scaling relations for Hall effect thrusters *J. Propul. Power* **27** 236–45
[17] Dankanich J W 2010 Low-thrust propulsion technologies, mission design, and application *Aerospace Technologies Advancements* ed T T Arif (Rijeka: InTech) pp 219–40
[18] Curran F M and Haag T W 1992 Extended life and performance test of a low-power arcjet *J. Spacecr. Rockets* **29** 444–52
[19] Fujita K and Arakawa Y 1999 Performance computation of a low-power hydrogen arcjet *J. Propul. Power* **15** 144–50
[20] Boulos M I, Fauchais P and Pfender E 1994 *Thermal Plasmas Fundamentals and Applications* (New York: Plenum)
[21] Heberlein J 2009 New approaches in thermal plasma technology *Pure Appl. Chem.* **74** 327–35
[22] Le Q H and Herdricht G 2013 Development of a 1 kW class thermal arcjet thruster TALOS *Proc. of the 33rd Int. Electric Propulsion Conf. (Washington, DC)* IEPC paper 2013–238
[23] Auweter-Kurtz M, Gölz T, Habiger H and Hammer F 1998 High-power hydrogen arcjet thrusters *J. Propul. Power* **14** 764–73
[24] Welle R 1997 Space propulsion applications of helium arcjets *Proc. of the 35th Aerospace Sciences Meeting and Exhibit (Reno, NV)* AIAA paper 97–0794
[25] Horisawa H and Kimura I 2000 Very low-power arcjet testing *Vacuum* **59** 106–17
[26] Choueiri E Y 1998 Scaling of thrust in self-field magnetoplasmadynamic thrusters *J. Propul. Power* **14** 744–53

[27] Myers R M, Mantenieks M A and Lapointe M R 1991 MPD thruster technology *Proc. of the Conf. on Advanced SEI Technologies (Cleveland, OH)* AIAA paper 1991–3568

[28] Nakata D, Toki K, Funaki I, Shimizu Y, Kuninaka H and Arakawall Y 2005 Experimental verification of the nozzle shape optimization for self-field MPD thruster *Proc. of the 29th Int. Electric Propulsion Conf. (Princeton, NJ)* IEPC paper 2005–163

[29] Hoyt R P 2005 Magnetic nozzle design for high-power MPD thrusters *Proc. of the 29th Int. Electric Propulsion Conf. (Princeton, NJ)* IEPC paper 2005–230

[30] Kuriki K and Suzuki H 1978 Transitional behavior of MPD arcjet operation *AIAA J.* **16** 1062–7

[31] Kubota K, Funaki I and Okuno Y 2005 Numerical investigation of ionization and acceleration process in a self-field MPD thruster *Proc. of the 29th Int. Electric Propulsion Conf. (Princeton, NJ)* IEPC paper 2005–089

[32] Kodys A D and Choueiri E Y 2005 A critical review of the state-of-the-art in the performance of applied-field magnetoplasmadynamic thrusters *Proc. of the 41st Joint Propulsion Conf. (Tucson, AZ)* AIAA paper 2005–4247

[33] La Pointe M R, Strzempkowski E and Pencil E 2004 High power MPD thruster performance measurements *Proc. of the 40th Joint Propulsion Conf. (Fort Lauderdale, Fl)* AIAA paper 2004–3467

[34] Choueiri E Y and Ziemer J K 2001 Quasi-steady magnetoplasmadynamic thruster performance database *J. Propul. Power* **17** 967–76

[35] Sovey J S, Vetrone R H, Grisnik S P, Myers R M and Parkes J E 1994 Test facilities for high-power electric propulsion *J. Propul. Power* **10** 18–24

[36] Tikhonov V B, Semenikhin S A, Brophy J R and Polk J E 1997 Performance of 130 kW MPD thruster with an external magnetic field and Li as a propellant *Proc. of the 25th Int. Electric Propulsion Conf. (Cleveland, OH)* IEPC Paper 1997–117

[37] Clark K E and Jahn R G 1970 Quasi-steady plasma acceleration *AIAA J.* **8** 216–20

[38] Choueiri E Y, Kelly A J and Jahn R G 1993 Mass savings domain of plasma propulsion for LEO to GEO transfer *J. Spacecr. Rockets* **30** 749–54

[39] Krülle G, Auweter-Kurtz M and Sasoh A 1998 Technology and application aspects of applied field magnetoplasmadynamic propulsion *J. Propul. Power* **14** 754–63

[40] Mikellides P G, Turchi P J and Roderick N F 1995 Theoretical model for applied field MPD thrusters *Proc. of the 31st Joint Propulsion Conf. (San Diego, CA)* AIAA paper 1995–2676

[41] Paganucci F, Rossetti P, Andrenucci M, Tikhonov V B and Obukhov V A 2001 Performance of an applied field MPD thruster *Proc. of the 27th Int. Electric Propulsion Conf. (Pasadena, CA)* IEPC paper 2001–135

[42] Boxberger A, Bambach P, Herdrich G and Fasoulas S 2012 Experimental investigation of steady-state applied-field magnetoplasmadynamic thrusters at Institute of Space Systems *Proc. of the 48th Joint Propulsion Conf.* (*Atlanta, GA*) AIAA paper 2012–4012

[43] Burton R L and Turchi P J 1998 Pulsed Plasma Thruster *J. Propul. Power* **14** 716–35

[44] Molina-Cabrera P, Herdrich G, Lau M, Fausolas S, Schoenherr T and Komurasaki K 2011 Pulsed Plasma Thrusters: a worldwide review and long yearned classification *Proc. of the 32nd Int. Electric Propulsion Conf. (Wiesbaden, Germany)* IEPC paper 2011–340

[45] Schönherr T 2016 Plasma acceleration in ablative pulsed plasma thrusters *Encyclopedia of Plasma Technology* ed J Leon Shohet (London: Taylor & Francis) (to be published)

[46] Rezaeiha A and Schönherr T 2014 Review of worldwide activities in liquid-fed pulsed plasma thruster *J. Propul. Power* **30** 253–64

[47] Koizumi H, Kakami A, Furuta Y, Komurasaki K and Arakawa Y 2003 Liquid propellant pulsed plasma thruster *Proc. of the 28th Int. Electric Propulsion Conf. (Toulouse, France)* IEPC paper 2003–87

[48] Gessini P, Habl L T C, Barcelos M N D Jr, Ferreira J L, Marques R I and Coletti M 2013 Low Power Ablative Pulsed Plasma Thrusters *Proc. of the 33rd Int. Electric Propulsion Conf. (Washington, DC)* IEPC paper 2013–344

[49] Spanjers G G, McFall K A, Gulczinski F S III and Spores R A 1996 Investigation of propellant inefficiencies in pulsed plasma thrusters *Proc. of the 32nd Joint Propulsion Conf. (Lake Buena Vista, FL)* AIAA paper 1996–2733

[50] Ziemer J K and Choueiri E Y 2001 Scaling laws for electromagnetic pulsed plasma thrusters *Plasma Sources Sci. Technol.* **10** 395–405

[51] Markusic T E, Polzin K A, Choueiri E Y, Keidar M, Boyd I D and Lepsetz N 2005 Ablative Z-pinch pulsed plasma thruster *J. Propul. Power* **21** 392–400

[52] Lovberg R H and Dailey C L 1982 Large inductive thruster performance measurement *AIAA J.* **20** 971–7

[53] Cassibry J T 2008 Comparison of directly and inductively coupled pulsed electromagnetic thrusters *IEEE Trans. Plasma Science* **36** 2180–8

[54] Keidar M *et al* 2005 Magnetically enhanced vacuum arc thruster *Plasma Sources Sci. Technol.* **14** 661–9

[55] Keidar M, Zhuang T, Shashurin A, Teel G, Chiu D, Lukas J, Haque S and Brieda L 2015 Electric propulsion for small satellites *Plasma Phys. Control. Fusion* **57** 014005

[56] Polk J E, Sekerak M J, Ziemer J K, Schein J, Qi N and Anders A 2008 A theoretical analysis of vacuum arc thruster and vacuum arc ion thruster performance *IEEE Trans. Plasma Sci.* **36** 2167–79

[57] Jimenez Diaz M, Garrigues L, Hagelaar G J M, Gaboriau F, Liard L, Herrero L and Blanchet A 2015 Study of a coaxial vacuum arc thruster plume and its interaction with applied magnetic field *Proc. of the 34th Int. Electric Propulsion Conf. (Hyogo-Kobe, Japan)* IEPC paper 2015–82

[58] Wilbur P J, Rawlin V K and Beattie J R 1998 Ion thruster development trends and status in the United States *J. Propul. Power* **14** 708–15

[59] Goebel D M, Wirz R E and Katz I 2007 Analytical ion thruster discharge performance model *J. Propul. Power* **23** 1055–67

[60] Groh K H and Loeb H W 1994 State of the art of radio-frequency ion sources for space propulsion *Rev. Sci. Instrum.* **65** 1741–4

[61] Chabert P, Arancibia Monreal J, Bredin J, Popelier L and Aanesland A 2012 Global model of a gridded-ion thruster powered by a radiofrequency inductive coil *Phys. Plasmas* **19** 073512

[62] Loeb H W 2005 Plasma-based ion beam sources *Plasma Phys. Control. Fusion* **47** B565–76

[63] Williams L T and Walker M L R 2013 Ion production cost of a gridded helicon ion thruster *Plasma Source Sci. Technol.* **22** 055019

[64] Loeb H W, Schartner K H, Meyer B K, Feili D, Weis St and Kirmse D 2005 Forty years of Giessen EP activities and the recent RIT-microthruster development *Proc. of the 29th Int. Electric Propulsion Conf. (Princeton, NJ)* IEPC paper 2005–031

[65] Leiter H J, Killinger R, Bassner H, Müller J, Kukies R and Fröhlich T 2003 Development and performance of the advanced radio frequency ion thruster RIT-XT *Proc. of the 28th Int. Electric Propulsion Conf. (Toulouse, France)* IEPC paper 2003–115

[66] Volkmar C and Ricklefs U 2015 Implementation and verification of a hybrid performance and impedance model of gridded radio-frequency ion thrusters *Eur. Phys. J.* D **69** 227

[67] Kuninaka H and Satori S 1998 Development and demonstration of a cathode-less electron cyclotron resonance ion thruster *J. Propul. Power* **14** 1022–6

[68] Kuninaka H, Nishiyama K, Funaki I, Yamada T, Shimizu Y and Kawaguchi J 2007 Powered flight of electron cyclotron resonance ion engines on Hayabusa explorer *J. Propul. Power* **23** 544–51

[69] Bramanti C, Izzoa D, Samaraeea T, Walker R and Fearn D 2009 Very high delta-V missions to the edge of the solar system and beyond enabled by the dual-stage 4-grid ion thruster concept *Acta Astronaut.* **64** 735–44

[70] Lieberman M A and Lichtenberg A J 1994 *Principles of Plasma Discharges and Materials Processing* (New York: Wiley)

[71] Lee C and Lieberman M A 1995 Global model of Ar, O_2, Cl_2, and Ar/O_2 high-density plasma discharges *J. Vac. Sci. Technol.* A **13** 368–80

[72] Brophy J R and Noca M 1998 Electric propulsion for Solar system exploration *J. Propul. Power* **14** 700–7

[73] Oh D Y 2007 Evaluation of solar electric propulsion technologies for discovery-class missions *J. Spacecr. Rockets* **44** 399–411

[74] Patterson M J, Pinero L and Sovey J S 2009 Near-term high power ion propulsion options for Earth-orbital applications *Proc. of the 45th Joint Propulsion Conf. (Denver, CO)* AIAA paper 2009–4819

[75] Patterson M J, Herman D, Shastry R, Van Noord J and Foster J E 2012 Annular-geometry ion engine: Concept, development status, and preliminary performance *Proc. of the 48th Joint Propulsion Conf. (Atlanta, GA)* AIAA paper 2012–3798

[76] Patterson M J, Thomas R E, Crofton M W, Young J A and Foster J E 2015 High thrust-to-power annular engine technology *Proc. of the 51st Joint Propulsion Conf. (Orlando, FL)* AIAA paper 2015–3719

[77] Kim V, Kozubsky K N, Murashko V M and Semenkin A V 2007 History of the Hall Thrusters Development in USSR *Proc. of the 30th Int. Electric Propulsion Conf. (Florence, Italy)* IEPC paper 2007–142

[78] Morozov A I and Savelyev V V 2000 Fundamentals of stationary plasma thruster theory *Reviews of Plasma Physics* vol 21, ed B B Kadomtsev and V D Shafranov (New York: Consultant Bureau) pp 203–391

[79] Kim V 1998 Main physical features and processes determining the performance of stationary plasma thrusters *J. Propul. Power* **14** 736–43

[80] Zhurin V V, Kaufmann H R and Robinson R S 1999 Physics of closed drift thrusters *Plasma Sources Sci. Technol.* **8** R1–20

[81] Gascon N, Dudeck M and Barral S 2003 Wall material effects in stationary plasma thrusters. I. Parametric studies of an SPT-100 *Phys. Plasmas* **10** 4123–36

[82] Choueiri E Y 2001 Fundamental difference between the two Hall thruster variants *Phys. Plasmas* **8** 5025–33

[83] Mazouffre S 2013 Laser-induced fluorescence diagnostics of the cross-field discharge of Hall thrusters *Plasma Sources Sci. Technol.* **22** 013001

[84] Lazurenko A, Vial A, Bouchoule A, Skrylnikov A, Kozlov V and Kim V 2006 Dual-mode operation of stationary plasma thrusters *J. Propul. Power* **22** 38–475

[85] Hofer R R and Jankovsky R S 2001 A Hall thruster performance model incorporating the effects of a multiply-charged plasma *Proc. of the 37th Joint Propulsion Conf. (Salt Lake City, UT)* AIAA Paper 2001–3322

[86] Koppel C R, Marchandise F, Prioul M, Estublier D and Darnon F 2005 The SMART-1 electric propulsion subsystem around the Moon: in flight experience *Proc. of the 41th Joint Propulsion Conf. (Tucson, Arizona)* AIAA paper 05–3671

[87] Gates M, Stich S, McDonald M, Muirhead B, Mazanek D, Abell P and Lopez P 2015 The Asteroid Redirect Mission and sustainable human exploration *Acta Astronaut.* **111** 29–36

[88] Choueiri E Y 2001 Plasma oscillations in Hall thrusters *Phys. Plasmas* **8** 1411–26

[89] Barral S and Ahedo E 2009 Low-frequency model of breathing oscillations in Hall discharges *Phys. Rev.* E **79** 046401

[90] Boeuf J P and Garrigues L 1995 Low frequency oscillations in a stationary plasma thruster *J. Appl. Phys.* **84** 3541–54

[91] Barral S, Makowski K, Peradzyński Z and Dudeck M 2005 Transit-time instability in Hall thrusters *Phys. Plasmas* **12** 073504

[92] Vaudolon J and Mazouffre S 2015 Observation of high-frequency ion instabilities in a cross-field plasma *Plasma Sources Sci. Technol.* **24** 032003

[93] McDonald M S, Bellanty C K, St. Pierrez B A and Gallimore A D 2011 Measurement of cross-field electron current in a Hall thruster due to rotating spoke instabilities *Proc. of the 47th Joint Propulsion Conf. (San Diego, CA)* AIAA paper 2011–5810

[94] Ellison C L, Raitses Y and Fisch N J 2012 Cross-field electron transport induced by a rotating spoke in a cylindrical Hall thruster *Phys. Plasmas* **19** 013503

[95] Tsikata S, Lemoine N, Pisarev V and Grésillon D M 2009 Dispersion relations of electron density fluctuations in a Hall thruster plasma, observed by collective light scattering *Phys. Plasmas* **16** 033506

[96] Tsikata S, Honoré C, Lemoine N and Grésillon D M 2010 Three-dimensional structure of electron density fluctuations in the Hall thruster plasma: $E \times B$ mode *Phys. Plasmas* **17** 112110

[97] Adam J C, Héron A and Laval G 2004 Study of stationary plasma thrusters using two-dimensional fully kinetic simulations *Phys. Plasmas* **11** 295–305

[98] Coche P and Garrigues L 2014 A two-dimensional (azimuthal-axial) Particle-In-Cell model of a Hall thruster *Phys. Plasmas* **21** 023503

[99] Janes G S and Lowder R S 1966 Anomalous electron diffusion and ion acceleration in a low-density plasma *Phys. Fluids* **9** 1115–23

[100] Meezan N B, Hargus W A Jr and Cappelli M A 2001 Anomalous electron mobility in a coaxial Hall discharge plasma *Phys. Rev.* E **63** 026410

[101] Koo J W and Boyd I D 2006 Modeling of anomalous electron mobility in Hall thrusters *Phys. Plasmas* **13** 033501

[102] Barral S, Makowski K, Peradzyński Z, Gascon N and Dudeck M 2003 Wall material effects in stationary plasma thrusters. II. Near-wall and in-wall conductivity *Phys. Plasmas* **10** 4137–52

[103] Ahedo E, Gallardo J and Martínez-Sánchez M 2003 Effects of the radial plasma-wall interaction on the Hall thruster discharge *Phys. Plasmas* **10** 3397–409

[104] Garrigues L, Hagelaar G J M, Boniface C and Boeuf J P 2006 Anomalous conductivity and secondary electron emission in Hall effect thrusters *J. Appl. Phys.* **100** 123301

[105] Ducrocq A, Adam J C, Héron A and Laval G 2006 High-frequency electron drift instability in the cross-field configuration of Hall thrusters *Phys. Plasmas* **13** 102111

[106] Héron A and Adam J C 2013 Anomalous conductivity in Hall thrusters: effects of the non-linear coupling of the electron-cyclotron drift instability with secondary electron emission of the walls *Phys. Plasmas* **20** 082313

[107] Mazouffre S, Pérez Luna J and Dannenmayer K 2007 Examination of plasma-wall interactions in Hall effect thrusters by means of calibrated thermal imaging *J. Appl. Phys.* **102** 023304

[108] Mazouffre S, Dannenmayer K and Blank C 2011 Impact of discharge voltage on wall-losses in a Hall thruster *Phys. Plasmas* **18** 064501
[109] Ahedo E 2002 Presheath/sheath model of a plasma with secondary emission from two parallel walls *Phys. Plasmas* **9** 4340–7
[110] Ahedo E and De Pablo V 2007 Combined effects of electron partial thermalization and secondary emission in Hall thruster discharges *Phys. Plasmas* **14** 083501
[111] Raitses Y, Staack D, Keidar M and Fisch N J 2005 Electron-wall interaction in Hall thrusters *Phys. Plasmas* **12** 057104
[112] Langendorf S and Walker M 2015 Effect of secondary electron emission on the plasma sheath *Phys. Plasmas* **22** 033515
[113] Cheng S and Martínez-Sánchez M 2008 Hybrid particle-in-cell erosion modeling of two Hall thrusters *J. Propul. Power* **24** 987–98
[114] Peterson P and Manzella D 2003 Investigation of the erosion characteristics of a laboratory Hall thruster *Proc. of the 39th Joint Propulsion Conf. (Huntsville, AL)* AIAA paper 2003–5005
[115] Keidar M, Boyd I D and Beilis I I 2004 Modeling of a high-power thruster with anode layer *Phys. Plasmas* **11** 1715–22
[116] Perez-Luna J, Hagelaar G J M, Garrigues L and Boeuf J P 2007 Model analysis of a double-stage Hall effect thruster with double-peaked magnetic field and intermediate electrode *Phys. Plasmas* **14** 113502
[117] Garrigues L, Boniface C, Hagelaar G J M and Boeuf J P 2008 Modeling of an advanced concept of a double stage Hall effect thruster *Phys. Plasmas* **15** 113502
[118] Ahedo E and Parra F I 2005 A model of the two-stage Hall thruster discharge *J. Appl. Phys.* **98** 023303
[119] Kuwano H, Ohno A, Kuninaka H and Nakashima H 2007 Development and thrust performance of a microwave discharge Hall thruster *Proc. of the 30th Int. Electric Propulsion Conf.* (*Florence, Italy*) IEPC paper 2007–085
[120] Mazouffre S, Bourgeois G, Dannenmayer K and Lejeune A 2012 Ionization and acceleration processes in a small, variable channel width, permanent magnet Hall thruster *J. Phys. D: Appl. Phys.* **45** 185203
[121] Smirnov A, Raitses Y and Fisch N J 2003 Enhanced ionization in the cylindrical Hall thruster *J. Appl. Phys.* **94** 852–7
[122] Raitses Y and Fisch N J 2001 Parametric investigations of a nonconventional Hall thruster *Phys. Plasmas* **8** 2579–86
[123] Seo M, Lee J, Seon J, Lee H J and Choe W 2013 Radial scale effect on the performance of low-power cylindrical Hall plasma thrusters *Appl. Phys. Lett.* **103** 133501
[124] Kim H, Lim Y, Choe W, Park S and Seon J 2015 Effect of magnetic field configuration on the multiply charged ion and plume characteristics in Hall thruster plasmas *Appl. Phys. Lett.* **106** 154103
[125] Courtney D G and Martínez-Sánchez M 2007 Diverging cusped-field Hall thruster (DCHT) *Proc. of the 30th Int. Electric Propulsion Conf. (Florence, Italy)* IEPC paper 2007–39
[126] Gildea S R, Martínez-Sánchez M, Nakles M R and Hargus W A Jr 2009 Experimentally characterizing the plume of a divergent cusped-field thruster *Proc. of the 31th Int. Electric Propulsion Conf. (Ann Arbor, MI)* IEPC paper 2009–259
[127] MacDonald N A, Young C V, Cappelli M A and Hargus W A Jr 2012 Ion velocity and plasma potential measurements of a cylindrical cusped field thruster *J. Appl. Phys.* **111** 093303
[128] Kornfeld G, Koch N and Harmann H P 2007 Physics and Evolution of HEMP-Thrusters *Proc. of the 30th Int. Electric Propulsion Conf. (Florence, Italy)* IEPC paper 2007–108
[129] Koch N *et al* 2001 The HEMPT concept—a survey on theoretical considerations and experimental evidences *Proc. of the 32nd Int. Electric Propulsion Conf. (Wiesbaden, Germany)* IEPC paper 2011–236
[130] Beal B E, Gallimore A D, Haas J M and Hargus W A 2004 Plasma properties in the plume of a Hall thruster cluster *J. Propul. Power* **20** 985–91
[131] Walker M L R and Gallimore A D 2007 Hall thruster cluster operation with a shared cathode *J. Propul. Power* **23** 528–36
[132] Florenz R and Gallimore A D 2011 Developmental status of a 100 kW class laboratory nested channel Hall thruster *Proc. of the 32nd Int. Electric Propulsion Conf. (Wiesbaden, Germany)* IEPC paper 2011–246
[133] Hall S J, Florenz R E, Gallimore A D, Kamhawi H, Brown D L, Polk J E, Goebel D M and Hofer R R 2014 Implementation and initial validation of a 100 kW class nested-channel Hall thruster *Proc. of the 50th Joint Propulsion Conf. (Cleveland, OH)* AIAA paper 2014–3815
[134] Mikellides I G, Katz I, Hofer R R, Goebel D M and DeGrys K 2011 Magnetic shielding of the channelwalls in a Hall plasma accelerator *Phys. Plasmas* **18** 033501
[135] Mikellides I G, Katz I, Hofer R R and Goebel D M 2013 Magnetic shielding of walls from the unmagnetized ion beam in a Hall thruster *Appl. Phys. Lett.* **102** 023509
[136] Mikellides I G, Katz I, Hofer R R and Goebel D M 2014 Magnetic shielding of a laboratory Hall thruster. I. Theory and validation *J. Appl. Phys.* **115** 043303
[137] Hofer R R, Goebel D M, Mikellides I G and Katz I 2014 Magnetic shielding of a laboratory Hall thruster. II. Experiments *J. Appl. Phys.* **115** 043304
[138] Mazouffre S, Vaudolon J, Largeau G, Hénaux C, Rossi A and Harribey D 2014 Visual evidence of magnetic shielding with the PPS-Flex Hall thruster *IEEE Trans. Plasma Sci.* **42** 2668–9
[139] Mikellides I G, Hofer R R, Katz I and Goebel D M 2014 Magnetic shielding of Hall thrusters at high discharge voltages *J. Appl. Phys.* **116** 053302
[140] Goebel D M, Hofer R R, Mikellides I G, Katz I, Polk J E and Dotson B 2013 Conducting wall Hall thrusters *Proc. of the 33rd Int. Electric Propulsion Conf. (Washington, DC)* IEPC paper 2013–276
[141] Mazouffre S, Tsikata S and Vaudolon J 2014 Development and experimental characterization of a wall-less Hall thruster *J. Appl. Phys.* **116** 243302
[142] Vaudolon J, Mazouffre S, Hénaux C, Harribey D and Rossi A 2015 Optimization of a wall-less Hall thruster *Appl. Phys. Lett.* **107** 174103
[143] Aanesland A, Mazouffre S and Chabert P 2011 PEGASES—a new promising electric propulsion concept *EuroPhys. News* **42** 28–31
[144] Aanesland A, Rafalskyi D, Bredin J, Grondein P, Oudini N, Chabert P, Levko D, Garrigues L and Hagelaar G 2015 The PEGASES gridded ion–ion thruster performance and predictions *IEEE Trans. Plasma Sci.* **43** 321–6
[145] Aanesland A, Bredin J, Chabert P and Godyak V 2013 Electron energy distribution function and plasma parameters across magnetic filters *Appl. Phys. Lett.* **102** 154107
[146] Rafalskyi D, Popelier L and Aanesland A 2014 Experimental validation of the dual positive and negative ion beam acceleration in the plasma propulsion with electronegative gases thruster *J. Appl. Phys.* **115** 053301
[147] Lafleur T, Rafalskyi D and Aanesland A 2015 Alternate extraction and acceleration of positive and negative

ions from a gridded plasma source *Plasma Sources Sci. Technol.* **24** 015005
[148] Renaud D, Gerst D, Mazouffre S and Aanesland A 2015 $E \times B$ probe measurements in molecular and electronegative plasmas *Rev. Sci. Instrum.* **86** 123507
[149] Chabert P and Braithwaite N 2011 *Physics of Radio-Frequency Plasmas* (Cambridge: Cambridge University Press)
[150] Charles C and Boswell R W 2012 Measurement and modelling of a radiofrequency micro-thruster *Plasma Sources Sci. Technol.* **21** 022002
[151] Stein W, Alexeenko A and Hrbud I 2008 Performance modeling of a coaxial radio-frequency gas-discharge microthruster *J. Propul. Power* **24** 1007–17
[152] Fruchtman A 2008 Energizing and depletion of neutrals by a collisional plasma *Plasma Sources Sci. Technol.* **17** 024016
[153] Greig A, Charles C, Paulin N and Boswell R W 2014 Volume and surface propellant heating in an electrothermal radio-frequency plasma micro-thruster *Appl. Phys. Lett.* **105** 054102
[154] Boswell R W and Chen F F 1997 Helicons—the early years *IEEE Trans. Plasma Sci.* **25** 1229–44
[155] Chen F F and Boswell R W 1997 Helicons—the past decade *IEEE Trans. Plasma Sci.* **25** 1245–57
[156] Charles C 2007 A review of recent laboratory double layer experiments *Plasma Sources Sci. Technol.* **16** R1–25
[157] Ahedo E and Martínez-Sánchez M 2009 Theory of a stationary current-free double layer in a collisionless plasma *Phys. Rev. Lett.* **103** 135002
[158] Charles C and Boswell R W 2003 Current-free double layer formation in a high-density helicon discharge *Appl. Phys. Lett.* **82** 1356–8
[159] Cohen S A, Siefert N S, Stange S, Bolvin R F, Scime E E and Levinton F M 2003 Ion acceleration in plasmas emerging from a helicon-heated magnetic-mirror device *Phys. Plasmas* **10** 2593–8
[160] Charles C and Boswell R W 2004 Laboratory evidence of a supersonic ion beam generated by a current-free helicon double-layer *Phys. Plasmas* **11** 1706–14
[161] West M D, Charles C and Boswell R W 2008 Testing a helicon double layer thruster immersed in a space-simulation chamber *J. Propul. Power* **24** 134–41
[162] Fruchtman A 2006 Electric field in a double layer and the imparted momentum *Phys. Rev. Lett.* **96** 065002
[163] Ahedo E 2011 Double-layer formation and propulsive assessment for a three-species plasma expanding in a magnetic nozzle *Phys. Plasmas* **18** 033510
[164] Takahashi K *et al* 2011 Direct thrust measurement of a permanent magnet helicon double layer thruster *Appl. Phys. Lett.* **98** 141503
[165] Pottinger S, Lappas V, Charles C and Boswell R W 2011 Performance characterization of a helicon double layer thruster using direct thrust measurements *J. Phys. D: Appl. Phys.* **44** 235201
[166] Williams L T and Walker M L R 2011 Thrust measurements of a helicon plasma source *Proc. of the 47th Joint Propulsion Conf. (San Diego, CA)* AIAA paper 2011–5893
[167] Takahashi K, Charles C, Boswell R and Ando A 2013 Performance improvement of a permanent magnet helicon plasma thruster *J. Phys. D: Appl. Phys.* **46** 352001
[168] Shabshelowitz A and Gallimore A D 2013 Performance and probe measurements of a radio-frequency plasma thruster *J. Propul. Power* **29** 919–29
[169] Sercel J C 1987 Electron-cyclotron-resonance (ECR) plasma acceleration *Proc. of the 19th Fluid Dynamics, Plasma Dynamics and Lasers Conf. (Honolulu, Hawaii)* AIAA paper 87–1407
[170] Jarrige J, Elias P Q, Cannat F and Packan D 2013 Performance comparison of an ECR plasma thruster using argon and xenon as propellant gas *Proc. of the 33rd Int. Electric Propulsion Conf. (Washington, DC)* IEPC paper 2013–420
[171] Jarrige J, Elias P Q, Cannat F and Packan D 2013 Characterization of a coaxial ECR plasma thruster *Proc. of the 44th Plasmadynamics and Lasers Conf. (San Diego, CA)* AIAA paper 2013–628
[172] Cannat F, Jarrige J, Lafleur T, Elias P Q and Packan D 2015 Experimental geometry investigation of a coaxial ECR plasma thruster *Proc. of the 34th Int. Electric Propulsion Conf. (Kobe-Hyogo, Japan)* IEPC paper 2015–242
[173] Cannat F, Lafleur T, Jarrige J, Chabert P, Elias P Q and Packan D 2015 Optimization of a coaxial electron cyclotron resonance plasma thruster with an analytical model *Phys. Plasmas* **22** 053503
[174] Chang Díaz F R 2000 The Vasimr rocket *Sci. Am.* **283** 90–7
[175] Chang Díaz F R 2001 An overview of the VASIMR engine: high power space propulsion with RF plasma generation and heating *AIP Conf. Proc.* **595** 3–15 *(Proc. of the 14th Topical Conf. on RF power in Plasmas (Oxnard, CA))*
[176] Arefiev A V and Breizman B N 2004 Theoretical components of the VASIMR plasma propulsion concept *Phys. Plasmas* **11** 2942–9
[177] Longmier B W *et al* 2011 VASIMR® VX-200 performance measurements and helicon throttle tables using argon and krypton *Proc. of the 32nd Int. Electric Propulsion Conf. (Wiesbaden, Germany)* IEPC paper 2011–156
[178] Olsen C S *et al* 2014 Investigation of plasma detachment from a magnetic nozzle in the plume of the VX-200 magnetoplasma thruster *IEEE Trans. Plasma Sci.* **43** 252–68
[179] York T M, Jacoby B A and Mikellides P 1992 Plasma flow processes within magnetic nozzle configurations *J. Propul. Power* **8** 1023–30
[180] Hooper E B 1993 Plasma detachment from a magnetic nozzle *J. Propul. Power* **9** 757–63
[181] Ahedo E and Merino M 2010 Two-dimensional supersonic plasma acceleration in a magnetic nozzle *Phys. Plasmas* **17** 073501
[182] Arefiev A V and Breizman B N 2008 Ambipolar acceleration of ions in a magnetic nozzle *Phys. Plasmas* **15** 042109
[183] Longmier B *et al* 2011 Ambipolar ion acceleration in an expanding magnetic nozzle *Plasma Sources Sci. Technol.* **20** 015007
[184] Merino M and Ahedo E 2015 Influence of electron and ion thermodynamics on the magnetic nozzle plasma expansion *IEEE Trans. Plasma Sci.* **43** 244–51
[185] Ahedo E and Merino M 2011 On plasma detachment in propulsive magnetic nozzles *Phys. Plasmas* **18** 053504
[186] Merino M and Ahedo E 2014 Plasma detachment in a propulsive magnetic nozzle via ion demagnetization *Plasma Sources Sci. Technol.* **23** 032001
[187] Kieckhafer A and King L B 2007 Energetics of propellant options for high-power Hall thrusters *J. Propul. Power* **23** 21–6
[188] Szabo J, Robin M, Paintal S, Pote B and Hruby V 2012 High density Hall thruster propellant investigations *Proc. of the 48th Joint Propulsion Conf. (Atlanta, GA)* AIAA paper 2012–3853
[189] Holste K, Gärtner W, Köhler P, Dietz P, Konrad J, Schippers S, Klar P J, Müller A and Schreiner P R 2015 In search of alternative propellants for ion thrusters *Proc. of the 34th Int. Electric Propulsion Conf. (Hyogo-Kobe, Japan)* IEPC paper 2015–320

[190] Singh L A and Walker M L R 2015 A review of research in low earth orbit propellant collection *Prog. Aerosp. Sci.* **75** 15–25

[191] Garrigues L 2012 Computational study of Hall-effect thruster with ambient atmospheric gas as propellant *J. Propul. Power* **28** 344–54

[192] Polzin K A, Peeples S R, Seixal J F, Mauro S L, Lewis B L, Jerman G A, Calvert D H and Dankanich J 2015 Propulsion system development for the iodine satellite (iSAT) demonstration mission *Proc. of the 34th Int. Electric Propulsion Conf. (Hyogo-Kobe, Japan)* IEPC paper 2015–09

[193] Szabo J, Pote B, Paintal S and Robin M 2012 Performance evaluation of an iodine-vapor Hall thruster *J. Propul. Power* **28** 848–57

[194] Marrese-Reading C *et al* 2005 The VHITAL program to demonstrate the performance and lifetime of a Bismuth-fueled very high Isp Hall thruster *Proc. of the 41st Joint Propulsion Conf. (Tucson, AZ)* AIAA paper 2005–4564

[195] Massey D, King L and Makela J 2008 Development of a direct evaporation Bismuth Hall thruster *Proc. of the 44th Joint Propulsion Conf. (Hartford, CT)* AIAA paper 2008–4520